Journal of Energy Systems (*JES*)

Quarterly Publishing Scientific Peer Reviewed Open Access Online Journal

The Journal of Energy Systems (JES) aims to publish high quality research and review papers on energy systems design and implementation. The submitted materials must fulfill the conditions of being innovative, sustainable and practical information to make an impact on the society of energy engineering.
First published in 2017

Content

Journal of Energy Systems (*JES*) *Volume 3, Issue 1*

Indexes

EBSCO Academic Search Ultimate

Fuzzy modeling of a hybrid solar dryer: experimental validation

Ahmed Zoukit

LSET, Applied Physics Department, FST, Cadi Ayyad University, Marrakesh, Morocco,
ahmed1991zoukit@gmail.com, ORCID: 0000-0001-5406-6038

Hicham El Ferouali

LSET, Applied Physics Department, FST, Cadi Ayyad University, Marrakesh, Morocco,
hichamelferouali@gmail.com. ORCID: 0000-0001-7541-4193

Issam Salhi

LSET, Applied Physics Department, FST, Cadi Ayyad University, Marrakesh, Morocco, isalhi@yahoo.fr.
ORCID: 0000-0001-8399-7827

Said Doubabi

LSET, Applied Physics Department, FST, Cadi Ayyad University, Marrakesh, Morocco, s.doubabi@ac.ma.
ORCID: 0000-0001-9947-5206

Naji Abdenouri

LSET, Applied Physics Department, FST, Cadi Ayyad University, Marrakesh, Morocco,
n.abdenouri@uca.ma. ORCID: 0000-0002-9399-5435

Abstract: A Takagi Sugeno fuzzy (TSF) modeling of an indirect hybrid solar-electrical dryer operated in forced convection (0.027 kg/s) was developed. The hybrid dryer was considered as a nonlinear and uncertain system where the operating point varies with weather conditions and airflow. The proposed TSF model was used to predict the drying temperature in no load conditions. Different experimental measurements were set up and used for evaluating the reliability of this model. At first and before applying this method to hybrid solar-electrical dryer, the TSF modeling was tested on solar mode and electrical mode where only one energy source was considered in each mode. The proposed model was experimentally validated in two main modes of the dryer operation: solar mode and electrical mode. The predicted behavior was closed to the experimental data with Root Mean Square Error (RMSE) of 2.34 and 2.21 in solar mode and electrical mode, respectively. The obtained predicted behavior confirms the pertinence of the identified model. The TSF model of the dryer leads to predict the drying temperature instantly with a huge reduction in simulation time in comparison with other modeling techniques. Thus, it is useful for synthesizing a control system of the drying parameters.

Nomenclature	
T_{ch}	Drying chamber temperature [°C]
T_a	Ambient temperature [°C]
G	Solar radiation [W/m^2]
P_g	Gas power [W]
$\dot{m}$	Airflow [kg/s]

1. INTRODUCTION

Solar energy is an important alternative source of energy. It is relatively preferred to other sources because it is free, abundant, inexhaustible and non-pollutant in nature compared with higher prices and shortage of fossil fuels [1,2].

Solar drying is one of the most potential applications. Farmers and citizen's dry food, fruits, seeds, medicinal plants and vegetables by spreading them in thin layers, on mats, paved ground or in the fields, thus exposing them to the sun. This process is not very hygienic, it depends on weather conditions and there is a risk of deterioration [3]. Some of the problems associated with open-air drying could be solved through the use of indirect solar dryers which can reduce crop losses and improve the quality of dried products [4]. According to the literature survey, different kinds of indirect solar dryers were constructed and investigated [5,6]. In the last configuration, the air was heated by a solar collector connected to a drying chamber. The products remain in shade and isolated from the sunlight and ambient air. The process occurred by the exchange of water from the wet products to the hot air.

The temperature inside the drying chamber is the most important parameter that affects directly the drying rate. Nevertheless, the fluctuating of weather conditions and the intermittency of solar energy highly affect the temperature threshold of drying air. Therefore, the quality of the dried products is strongly affected. Hence, solar dryers are still limited and could not be effective without the presence of another energy source and without control of all drying parameters (temperature, humidity and airflow).

Hybrid solar-electrical dryers are operating with a solar energy and electrical power as a secondary energy source. According to literature survey, many works [7, 8, 9, 10] used heat resistors inside the drying cells in order to maintain the drying temperature in a suitable range with high efficiency of heat energy exchange.

For efficient controlling system, predicting values of the output parameters related to input conditions is necessary [11]. It is represented by a predictive model of the system. The prediction of drying temperature can be established using several models based on heat transfer, movement and mass equation. These models require a hug computational time compared with the settling time of the dryer.

In previous works, solar dryers were modeled using various techniques [12]: artificial neural networks, Adaptive Neuron-Fuzzy Inference System (ANFIS), FUZZY, thermal modeling, mathematical modeling and drying kinetics model, etc. But, there is no literature found in modeling hybrid solar dryers by using model which can provide predictive output in enough less time to permit the complete control of temperature inside dryer.

Fuzzy logic modeling is based on input and output data, applied on nonlinear multi-inputs and multi-outputs systems [13,14]. The strength of fuzzy logic is the accuracy of output prediction even if the system is nonlinear and the input parameters are floating. Fuzzy modeling and fuzzy sets are widely used for predictions and estimations of floating and nonlinear parameters as reported in [15-17]. The behavior of solar dryer remains nonlinear in widely operated cases.

In all previous works, Fuzzy model was used only for modeling solar dryers supplied by solar irradiation without secondary energy source and only for the specific product drying [18-21]. This technique was used to predict the drying behavior taking into account different weather conditions, mainly ambient temperature, solar radiation, and relative humidity [18]. A fuzzy model was also developed to determine and calculate the temperature and moisture of jiggery during the evaporation of water content in a greenhouse system [19]. On the other hand, prediction models in no load conditions would provide thermal behavior of the dryer. Based on this, suitable range of products of interest will be specified for

the effective drying. In order to predict the greenhouse air temperature and relative humidity, an ANFIS prediction model of a greenhouse dryer in no load conditions was proposed in [20]. Authors in [21] proposed no load performances index for various solar dryers.

The main contribution of this paper is to perform an alternative method for modeling a hybrid solar-electrical dryer in no load conditions by using Takagi-Sugeno fuzzy (TSF) system. This method has never been explored for modeling hybrid dryers. The nonlinear system is linearized into different operating points. Then, linear models corresponding to every operating point are established. The fuzzy model is described by a family of fuzzy IF-THEN rules where each one represents a linear input-output relation of the system. The global fuzzy model of the studied dryer was achieved by smoothly blending these linear models together through the fuzzy membership functions in order to give the overall nonlinear behavior of the dryer.

The principal objective of this work is to develop a TSF model of hybrid solar-electrical dryer in order to predict accurately and quickly its thermal behavior in forced convection and in two operating modes: solar mode (energy was only provided by solar energy) and electrical mode (energy was only provided by electrical power). Fuzzy rules of the system were obtained based on experimental measurements of drying temperature at various solar radiations and electrical powers. Some simple linear models for several operating points were identified using Matlab system identification Toolbox (Ident) and were used to build the global TSF model of the studied dryer. Then, the developed model was experimentally validated at various solar radiation, ambient temperatures and electrical powers.

2. DESCRIPTION of EXPERIMENTAL SETUP

The solar dryer consists mainly of a solar collector where the air used in the drying process was heated and a drying chamber where the material to be dried was spread in tray, electrical fan allowing the choice of the desired airflow, resistance heater (4kW: accuracy +/- 2%) and an analogue power controller. The solar collector is a finned absorber (Length = 2m and Width = 1m) made from aluminum. The top side of the absorber is painted with matt black glycerophtalic lacquer (absorptivity = 0.95 and emissivity = 0.8). The number of fins is 24 and they are made from aluminum with 1mm thickness. The top losses are minimized by placing a glass cover of 3 mm thickness with a distance of 50 mm over the top of the absorber. The collector is stationary and inclined at a tilt angle of 30° (respect to the latitude of Marrakesh, Morocco) with the horizontal facing south all the duration of experiments. The bottom and sides are isolated with glass wool 40 mm thick. The solar collector is combined directly to the drying chamber without using any air conducts. The drying chamber was built from a steel structure. The walls were made from steel sheet metal and were isolated by mineral fiber 40 mm thick. The total capacity of the drying chamber is four mesh trays with a drying area of $0.94m^2$ (Figure 1).

Figure 1. Photo of an indirect hybrid solar-electrical dryer.

Figure 2 shows a schematic layout of the hybrid indirect solar-electrical dryer.
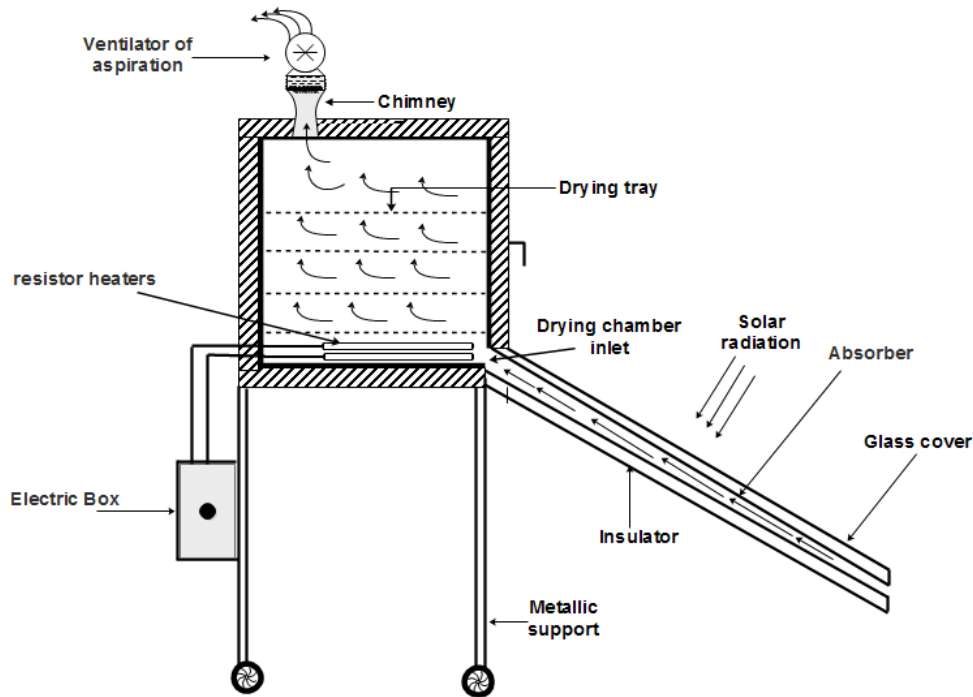
Figure 2. Bloc diagram of the hybrid solar dryer.

3. MATERIALS and METHODS

The dryer was unloaded because the investigations in no load conditions provide consistent results as they are not influenced by the type, the composition and the moisture content of food products. The experiments were conducted during several days starting at 11:00 am and finished at 13:30 pm. During this period, solar radiation and ambient temperature can be assumed constants. The dryer was placed in an unshaded and clear area during the whole duration of experiments. A fan was fixed in the chimney of the dryer to ensure an even distribution of air and also to exhaust the humidity of the product to the surrounding. In solar drying process, the drying air temperature changes with the magnitude of solar radiation. Thus, the auxiliary electric heater was used to adjust the drying air temperature. The preliminary heated drying air by solar radiation, arrived to the inlet of cabinet dryer will be heated by electrical resistance. The power of the electrical resistance was varied using an analogue power controller (037N0057, Danfoss). The drying air is then aspired by the exhaust fan of 10 cm diameter (Orion 12HBVXC model, 43W power input, running at 5000 rpm and volumic flow at 0.107 m^3/s). The fan was controlled by an Arduino Uno for maintaining an air flow of 0.027 kg/s. Temperature, humidity and solar radiation were recorded every 10 min. Temperature was measured and recorded at different locations inside the drying chamber (bottom, middle and the top) using temperature sensors type (TM-110 pt100, 0.5°C accuracy). Hygrometer sensors (HM-110, 0.5% accuracy) were employed for measuring the ambient relative humidity. Incident global solar radiation was measured during the experiments by a Keep and Zonnen pyranometer with a sensitivity of 14.69 10^{-3}. Velocity of drying air was measured using an anemometer (Kimo model CTV-210-BOS, 0.03 m/s accuracy) at the exit of the exhaust fan.

4. NON LINEARITY OF THE HYBRID DRYER

Experimental measurements of the temperature profile inside the drying chamber at three planes; top, middle and bottom were conducted in forced convection. It is noticed that there is no significant differences in average temperature (maximum difference of 1.4°C) at all planes due to the air vortex inside the drying chamber. However, only the average temperature of the drying chamber was considered for modeling.

The hybrid dryer is a complex nonlinear system. In order to figure out the nonlinear relationship of the dryer's input/output and to investigate its overall behavior, static characteristics of the dryer operated in solar mode and electrical mode were established based on experimental studies. The static characteristics lead also to easily identify the linear zones and the operating points of the dryer.

Static characteristics were built measuring the drying chamber temperature in steady state on the basis of solar radiation and electrical power of the resistance heater. From the conducted tests for different solar radiations (solar radiations and ambient temperatures are considered approximately constant from 11:00 am to 13:30 pm, for each day), the steady state was reached after two hours and a half (at about 13:30 pm).

Figure 3 depicts the static characteristics of the dryer operated in solar mode (Figure 3a) and electrical mode (Figure 3b). The plots clearly show the strong static non linearity of the dryer by appearance of saturation of the output for high solar radiations. To overcome this problem, the static characteristics of the dryer were divided into linear zones numbered (1, 2, 3, 4) and (1', 2', 3', 4') corresponding to different weather conditions (windy day, cloudy day, partly cloudy day and clear day) and electrical powers (low power, medium power, high power and very high power). Several operating points were singled out in the linear zones and linear models corresponding to each operating point were identified. A TSF model was developed to ensure the connection between the linear zones by combining the linear models to give the overall nonlinear behavior of the studied hybrid dryer.
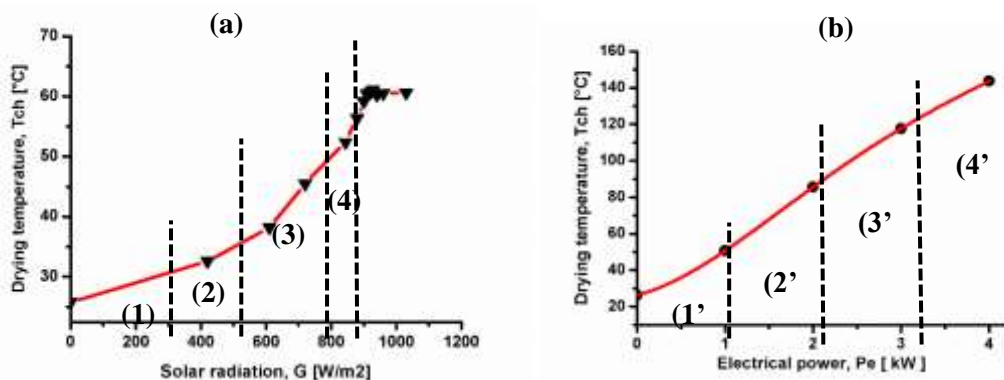
Figure 3. Static characteristics of the hybrid dryer, (a) solar mode; (b) electrical mode.

5. RESULTS AND DISCUSSIONS

5.1. Behavior of the dryer operated in solar mode

In order to identify the linear models corresponding to each operating point of the dryer operated in solar mode, several measurements were carried out in winter season for days December 12th, 16th, 2016 and January 5th, 18th, 2017 at different weather conditions. The dryer remains previously in shade and

immediately exposed to solar radiation for two hours and a half starting at 11:00 am. The highest air temperature inside the drying chamber was previously noticed between 11:00 am and 13:30 pm.

In clear days, the highest reached drying temperature was 50.2°C under a solar radiation of 964.4 W/m^2 for an ambient temperature of 25.6°C (Figure 4a) (measurements corresponding to the operating point in the linear zone 4), and 47.2°C at a solar radiation of 804.5W/m^2 (zone 3) and 25.1°C ambient temperature (Figure 4b). In a cloudy day (Figure 4c), the drying chamber temperature reached 42.2°C, under a solar radiation and ambient temperature of 630.6W/m^2 and 23.6°C, respectively (Zone 2).

Experimental tests were also conducted in a period of stormy weather and air temperature inside the drying chamber reached 14.2°C at a solar radiation of 101.3W/m^2 (Zone 1) and an ambient temperature of 12.1°C as shown in (Figure 4d).
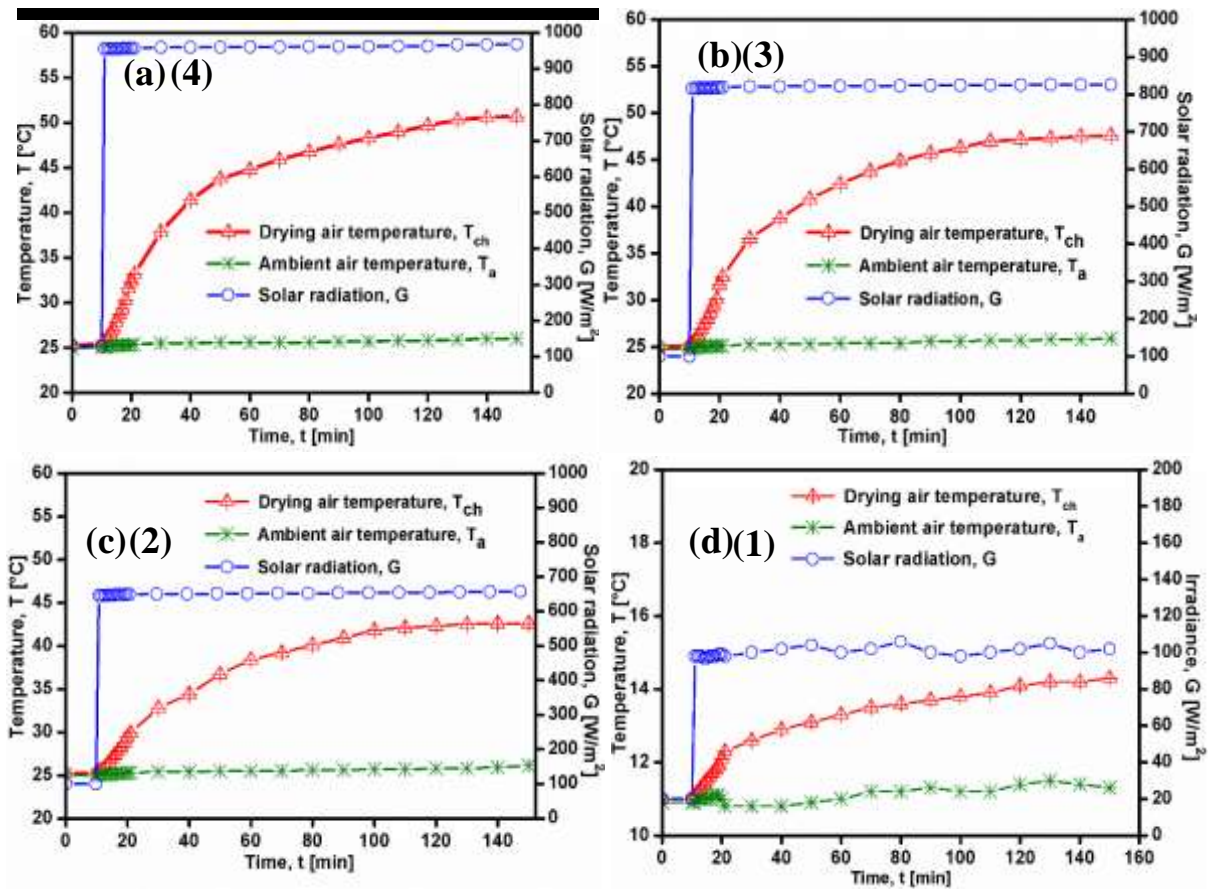
Figure 4. Solar intensity and air temperature variation; (a)(b) clear days, (c) windy day, (d) cloudy day. (1), (2), (3), (4) numbers corresponding to linear zones in static characteristic of the dryer in solar mode.

5.2. Behavior of the dryer operated in electrical mode

To identify the linear models corresponding to each operating point of the dryer operated in electrical mode, different measurements were carried out for days January 1st, 3rd, 7th, and 10th, 2017 at different electrical powers. The tests were conducted at night in the absence of solar radiation. The steady state was achieved in one hour of operation.

The drying temperature reached 37.4°C at an electrical power of 0.5kW and an ambient temperature of 24.6°C (Figure 5a (Zone 1')). At an electrical power of 1.5kW, the temperature reached 69.7°C at an ambient temperature of 22.6°C (Figure 5b (zone 2')). The average temperature inside the drying

chamber reached 100.1°C and 128.7°C at electrical powers of 2.5kW and 3.5kW and ambient temperatures of 21.5°C and 23.8°C, respectively as shown in Figures 5c,5d (zone 3',4').
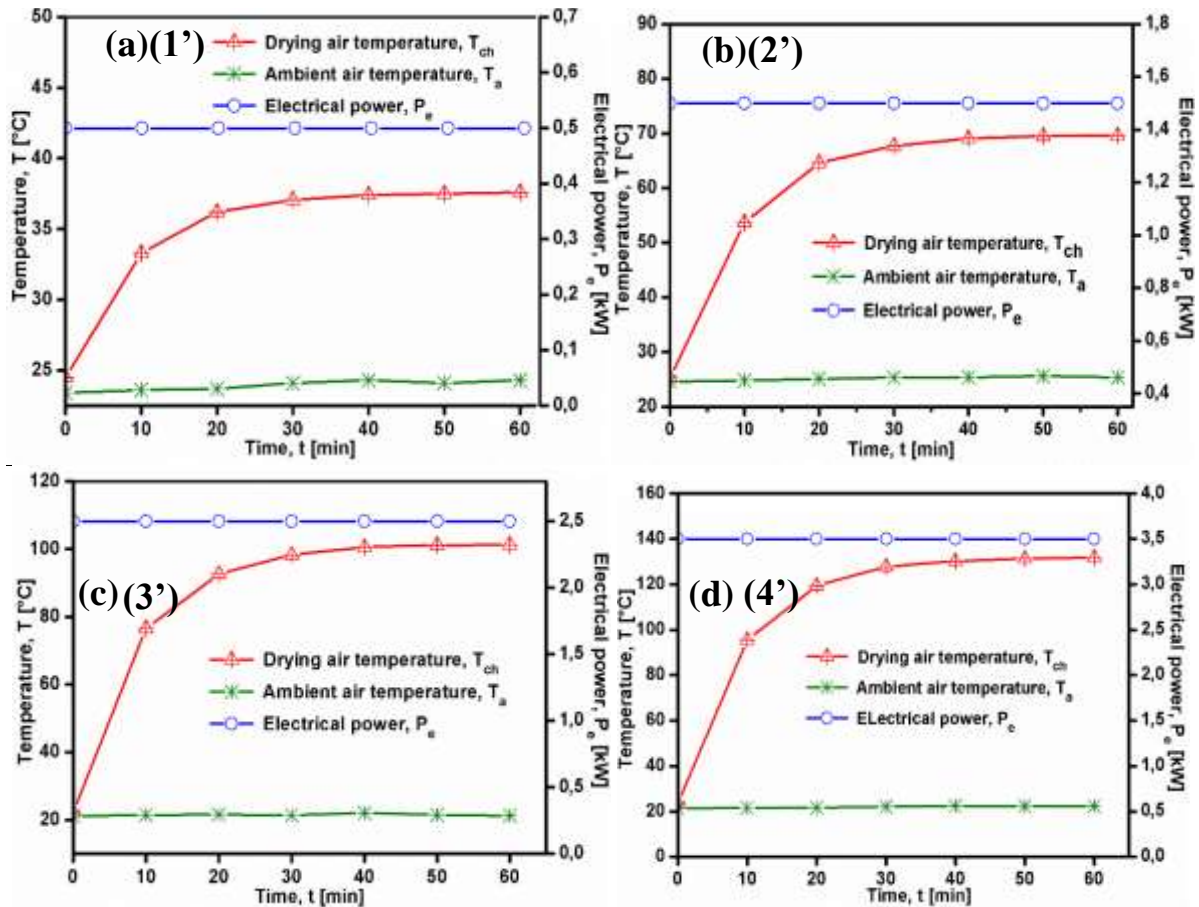
Figure 5. Electrical power and air temperature variation; (a) 0.5kW (b) 1.5kW, (c) 2.5kW, (d) 3.5kW. (1'), (2'), (3'), (4') numbers corresponding to linear zones in static characteristic of the dryer in Electrical mode.

6. HYBRID SOLAR-ELECTRICAL DRYER MODELING

6.1. The linear hybrid dryer models

The hybrid dryer dynamic response can be represented by different linear models depending on the operating points in the three operating modes (solar mode, electrical mode and hybrid mode).

The experimental measurements corresponding to different operating points led to highlight the influence of different inputs (solar radiation, ambient temperature and electrical power) on the behavior of the dryer. In addition, they permit to evaluate the simplest representation (linear models) of the dryer. In order to identify the linear models, the measured inputs and outputs were loaded into system identification Toolbox of Matlab environment using (Ident). This latter provides functions and Simulink blocs for constructing mathematical models based on least squares methods of dynamic systems from measured input/output data. In the three operating modes, the obtained response is similar to that of a second order system (Eq. [1]) with a best fitting of 96.5% where the parameters change according to each considered operating points.

$$F(s) = \frac{as + b}{s^2 + cs + d} \qquad (1)$$

The coefficients (a, b, c, d) are the linear model's parameters. These coefficients were computed using the measured data obtained for different solar radiations and electrical powers. Table 1 gives the identified coefficients of the linear models transfer functions. According to Table 1, the nonlinear evolution of coefficient (a, b, c, d) can be noticed, which confirms the high nonlinearity of the studied system. It confirms that it is impossible to represent the hybrid solar dryer by a unique second order model for different weather conditions and operating modes. To overcome this issue a TSF system was developed to obtain a global nonlinear model of the studied hybrid dryer.

Table 1. Linear models' parameters based on solar radiation and electrical power.

		Coefficients of linear models			
		a	b	c	d
Solar mode	964.7W/m^2 25.6°C	$1,919.10^{-5}$	$6,033.10^{-9}$	0,001273	2,048
	804.5 W/m^2 25.1°C	$2,543.10^{-5}$	$3,3.10^{-8}$	0,003218	$1,165.10^{-6}$
	463.6W/m^2 23.6°C	$2,878.10^{-5}$	$2,226.10^{-8}$	0,002761	$7,518.10^{-7}$
	251.2W/m^2 20.1°C	$3,104.10^{-5}$	$2.053.10^{-8}$	0.002662	$5.535.10^{-7}$
Electrical mode	0.5kW 24.6°C	34.7	24.7	2.027	0.9491
	1.5kW 22.6°C	39.7	20.68	1.82	0.65
	2.5kW 21.5°C	42.5	16.3	1.53	0.48
	3.5kW 23.8°C	45.2	14.2	1.21	0.41

6.2. Takagi Sugeno Fuzzy model of the hybrid dryer

In this paper, a TSF modeling based on linear functions of input variables was considered. It can approximate nonlinear systems with few rules and higher modeling accuracy [22, 23]. This model was used in many works and for many applications, where the linear models are used individually and aids for validating and interpretation of the global model [24, 25]. The TSF model combines all the linear models in order to find a global model of the system able to generate the appropriate output as shown in Figure 6.
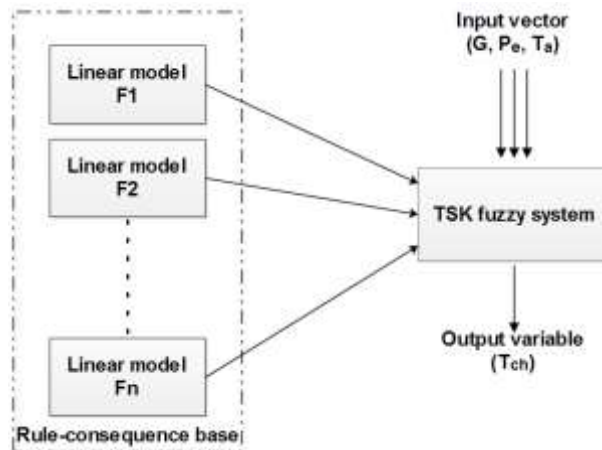
Figure 6. Structure of TSK fuzzy system

The TSF fuzzy system was built from the input/output and the obtained parameters of linear models. Figure 7 shows the seven membership functions corresponding to the dryer parameter (*G*) characterizing solar radiation. It can be seen that the generation of membership functions was focused in the high and low solar radiations where the system represents strong nonlinearity. The generated membership functions corresponding to the dryer parameter (*P$_e$*) characterizing the electrical power are shown in Figure 8. Figure 9 illustrates the generating membership functions corresponding to ambient temperature (*T$_a$*).
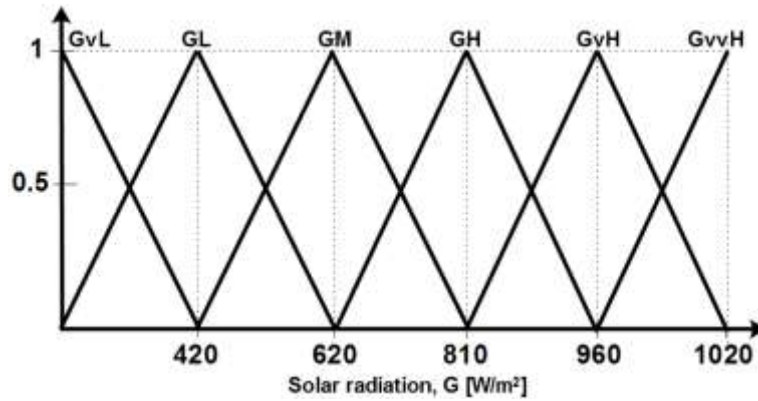
Figure 7. Membership function for solar radiation. (GvL): Irradiance Very low; (GL): Irradiance Low; (GM); Irradiance medium; (GH): Irradiance High; (GvH): Irradiance very High; (GvvH): Irradiance very very High.
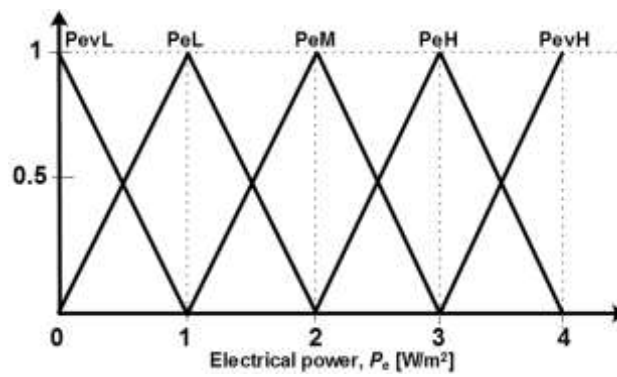
Figure 8. Membership function for electrical power. (PevL): Power Very low; (PeL): Power Low; (PeM); Power medium; (PeH): Power High; (PevH): Power very High.
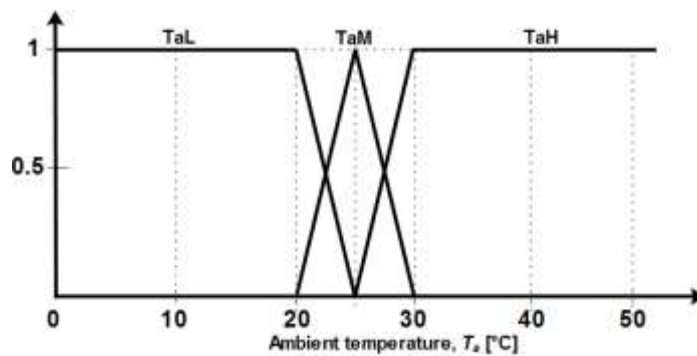
Figure 9. Membership function for ambient temperature. (Tal): Temperature Low; (TaM); Temperature medium; (TaH); Temperature High.

The rule of fuzzy model type Takagi Sugeno are built by the parameters of linear model. Where, each rule represents the parameters of a linear model corresponding to a specific operating point. Thus, the global fuzzy system gives the overall nonlinear behavior of the dryer system.

Using the fuzzy rules, the appropriate TSF model's output (drying temperature) was estimated according to the associated linear models as shown in Figure 10.
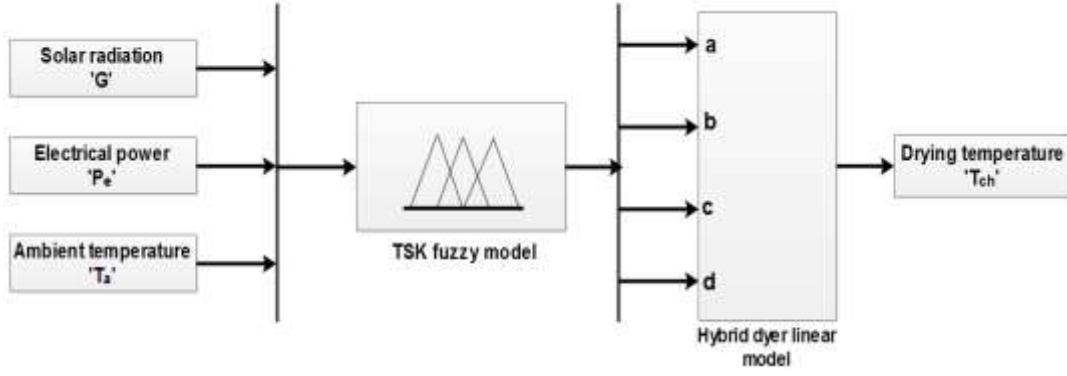
Figure 10. TSK fuzzy model of the hybrid solar-electrical dryer

The rules of the TSF fuzzy models are the following forms [22, 26]:

Rule i:

L_i: if x_1 is α_{i1}, x_2 is α_{i2}, …, and x_p is α_{ip} then F_i.

Where, L_i (i=1, 2, ..., n) is i-th fuzzy rule, x_j (j=1, 2, …, p) is input variable and F_i are output parameters of linear models obtained by L_i, α_{ij} (j = 1...p) is the fuzzy set of the variable inputs j.

Given the input $x_1^0, x_2^0, ..., x_j^0, x_m^0$ the global parameters F can be inferred by a weighted average defuzzification as Eq. [2]

$$F = \frac{\sum_{i=1}^{n} w_i F_i}{\sum_{i=1}^{n} w_i} \qquad (2)$$

Where the weight w_i implies the overall truth value of the premise of the j-th implication for the input, and is calculated as Eq. [3].

$$w_i = \prod_{j=1}^{m} \mu_{\alpha_i}(x_j) \qquad (3)$$

Where $\mu_{\alpha_i}(x_j)$ the grade of the membership function of xj in fuzzy set αi and it is characterized by a Gaussian function as Eq. [4].

$$\mu_{\alpha_i}(x_j) = \exp(-\frac{\left(x_j - c_i^j\right)^2}{b_i^j}) \qquad (4)$$

The application of TSF modeling provides an estimation of the dryer behavior for all combinations of solar radiation, ambient temperature and electrical power. This implies that for any weather condition and operating mode (solar mode, electrical mode and hybrid mode) the TSF fuzzy model will predict accurately the drying chamber temperature.

7. EXPERIMENTAL VALIDATION OF THE HYBRID DRYER TSF MODEL

The reliability and the performances of the developed model for describing the behavior of the hybrid dryer at three mains operating modes were evaluated by comparing the predicted drying temperature

with experimentally measured temperature during the operation of the dryer in solar mode, electrical mode and hybrid mode.

Experimental tests were performed in winter season, in clear days, cloudy days and at nights. The dryer was operated in forced convection at an airflow maintained at 0.027 kg/s.

7.1. Solar mode

Experimental measurements were conducted for days 2nd, 14th, January 2017 in a clear and cloudy weather. The average recorded solar radiations and ambient temperatures were 1014W/m², 24.5°C.
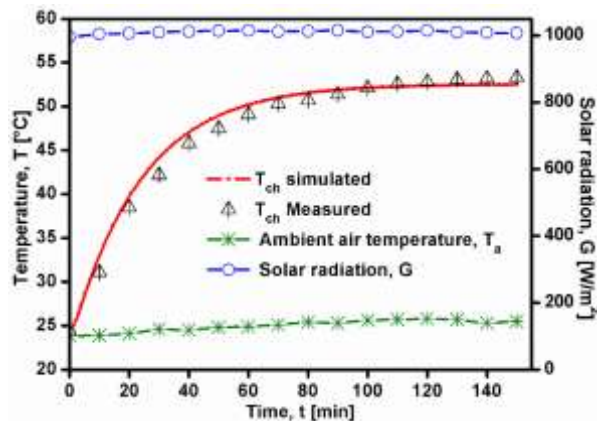
Figure 11. Validation of the constructed TSK model of the dryer operated in solar mode; average solar radiation of 1014.3W/m².

The predicted responses of the model were compared with the experimental ones as shown in Figure 11. It is clearly the measured temperature and the simulated one are in good accordance with an RMSE equal 2.34.

7.2. Electrical mode

In order to test the reliability of the constructed model for dryer operated in electrical mode, experimental measurements were conducted for day 10th, February 2017 at night. The considered electrical powers were 2kW (Figure 12) with ambient temperatures of 25.6°C.
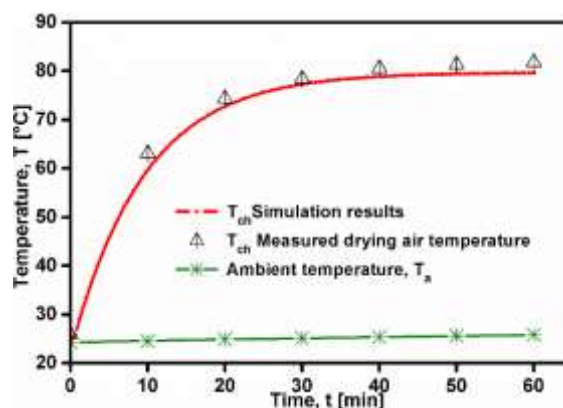
Figure 12. Validation of the constructed TSK model of the dryer operated in electrical mode; average electrical power of 2kW.

The predicted response was compared with the experimental ones as shown in Figure 11. It is clearly shown that the fit of drying temperature by the simulated ones is significantly good with an RMSE equal 2.21.

In Table 2 the values of RMSE of modeling the hybrid dryer operated in solar and electrical mode are presented.

Table 2. Root mean square error (RMSE) of modeling the hybrid dryer.

Operating mode	RMSE
Solar mode	2.34
Electrical mode	2.21

8. CONCLUSION

In this study, a hybrid solar-electrical dryer modeling operated in forced convection was investigated. A TSF model of the hybrid dryer was developed in order to describe its behavior in three mode of operation (solar mode, electrical mode and hybrid mode) in no load conditions. Static characteristics of the dryer were established to testify the strong nonlinearity of the dryer. The proposed TSF model was explored to predict nonlinear thermal behavior (drying temperature) of the dryer taking into account different solar radiations, ambient temperature, and electrical powers as input parameters. The TSF model was successfully validated through experimental tests with a RMSE of 2.34 and 2.21 for the dryer operated in solar mode and electrical mode, respectively. The proposed TSF model reveals a high prediction ability of the hybrid dryer with a huge reduction in simulation time comparing to other modeling methods. The proposed model will be useful for synthesizing the temperature controller and increasing the efficiency of the dryer to enhance the quality of the dried products. The system could be enhanced by adding a thermal energy storage such as pebbles or rock salts which can help to extend the drying time and also reduce the electrical consumption. Also for the area far from the electricity, the dryer cannot be operated, for this reason a PV models should be used. All this issues will be taken into considerations in future works.

Acknowledgment

REFERENCES

[1] Frakas, I, Seres, I, Meszaros, C. Analytical and experimental study of a modular solar dryer. Renewable energy 1999; 16: 773-778. DOI: https://doi.org/10.1016/S0960-1481(98)00278-X.

[2] Belloulid, M, O, Hamdi, H, Mandi, L, Ouazzani, N. Solar drying of wastewater sludge: a case study in Marrakesh, Morocco. Environmental Technology (United Kingdom) 2018; 0(0): 1–7. DOI: 10.1080/09593330.2017.1421713.

[3] Chan, Y, Dyah, N, Abdullah, K. Performance of a recirculation type integrated collector drying chamber (ICDC) solar dryer. Energy Procedia 2015; 68: 53-59. DOI: https://doi.org/10.1016/j.egypro.2015.03.232.

[4] Lopez-Vidana, E, C, Mendez-Lagunas, LL, Rodriguez-Ramirez, J. Efficiency of a hybrid solar-gas dryer. Solar energy 2013; 93: 23-31. DOI: https://doi.org/10.1016/j.solener.2013.01.027.

[5] Kumar, A, Singh, R, Prakash, O. Review of global solar drying status. Agric. Eng. Int 2014; 16.

[6] Prakash, O, Kumar, A, Laguri, V. Performance of modified greenhouse dryer with thermal energy storage. Energy reports 2016; 2: 155-162. DOI: https://doi.org/10.1016/j.egyr.2016.06.003.

[7] Boughali, S, Benmoussa, H, Bouchekima, B, Mennouche, D, Bouguettaia, H, Bechki, D. Crop drying of an indirect active hybrid Solar-Electrical dryer in eastern Algerian Septentrional Sahara. Solar energy 2009; 83: 2223-2232. DOI: https://doi.org/10.1016/j.solener.2009.09.006.

[8] Alejandro, R, Andrea, M, Francisco, C, Pedro, H. Mushroom dehydration in a hybrid solar dryer. Energy conversion and management 2013; 70: 31-39. DOI: https://doi.org/10.1016/j.enconman.2013.01.032.

[9] Augustus Leon, M, Kumar, S. Design and performance evaluation of a solar assisted biomass drying system with thermal storage. Drying technology 2008; 26: 936-947. DOI: https://doi.org/10.1080/07373930802142812.

[10] Ferreira, A, G, Charbel, A, L, T, Peres, R, L, Silva, J, G, Maia, C, B. Experimental analysis of a hybrid dryer. Thermal engineering 2007; 6: 03-07.

[11] Onat, M, Koten, H, Celik, H. Constant Temperature Control with a Fast Transient Response for a Gel Card Incubator, 6th Eur. Conf. Ren. Energy Sys. 25-27 June 2018, Istanbul, Turkey.

[12] Prakash, O, Laguri, V, Pandey, A, Kumar, A. Review on various modelling techniques for the solar dryers. Renew. Sustain. Energy Rev 2016; 62: 396-417. DOI: https://doi.org/10.1016/j.rser.2016.04.028.

[13] Seo, S, Kim, Y, Choi, H, H. Model predictive controller design for boost DC – DC converter using T – S fuzzy cost function. Int. J. Electron 2017; 104: 838–1853. DOI: https://doi.org/10.1080/00207217.2017.1329945.

[14] Tatli, H, ŞEN, Z. Prediction of Daily Maximum Temperatures Via Fuzzy Sets. Turkish Journal of Engineering and Environmental Sciences 2014; 25 (1): 1-9.

[15] Ibrahim, S. A, Ahmet Sahiner, A, Ibrahim, A. A. Fuzzy Logic Modeling for Prediction of the Nuclear Tracks; Journal of Multidisciplinary Modeling and Optimization 2018; 1: 33-40.

[16] Tütmez, B, Tercan, E. Use of Fuzzy Modeling Approach in Grade Estimation; Scientific Mining Journal 2006; 45: 39-47.

[17] Laouafi, A, Mordjaoui, M, Boukelia T, E. An adaptive neuro-fuzzy inference system-based approach for daily load curve prediction. Journal of energy system 2018; 2(3): 115-126.

[18] Prakash, O, Kumar, A, ANFIS modelling of natural convection greenhouse drying system for jiggery: an experimental validation. Int. J. Sustain. Energy 2014; 33: 316-335. DOI: https://doi.org/10.1080/14786451.2012.724070.

[19] Prakash, O, Kumar, A, Kaviti, AK, Kumar, PV. Prediction of the rate of moisture evaporation from jiggery in greenhouse drying using the fuzzy logic. Heat Transf. Res 2015; 46.

[20] Prakash, O, Kumar, A. ANFIS prediction model of a modified active greenhouse dryer in no-load condition in the month of January. Int. J. Adv.Comput. Res 2013; 3: 220-223.

[21] Singh, S, Kumar, S. Testing method for thermal performance based rating of various solar dryer designs. Solar energy 2012; 86: 87-98. DOI: https://doi.org/10.1016/j.solener.2011.09.009.

[22] Takagi, T, Sugeno, M. Fuzzy identification of systems and its applications to modeling and control. IEEE trans 1985; 15: 116-132. DOI: 10.1109/TSMC.1985.6313399.

[23] Zhu, B, He, CZ, Liatsis, P, Li, XY. A GMDH-based fuzzy modeling approach for constructing TS model. Fuzzy Sets Syst 2012 ; 189 : 19-29. DOI: https://doi.org/10.1016/j.fss.2011.08.004.

[24] Du, H, Zhang, N. Application of evolving Takagi-Sugeno fuzzy model to linear system identification. App. Soft Comput J 2008; 8: 676-686. DOI: 10.1016/j.asoc.2007.05.006 .

[25] Johansen, T, Shorten, R, Murray-Smith, R. On the interpretation and identification of dynamic (Takagi-Sugeno) fuzzy models. IEEE transaction 2000; 8: 297-313. DOI: 10.1109/91.855918.

[26] El Hamdaoui, A, Salhi, I, Belattar, A, Doubabi, S. Modeling a three-phase micro hydropower plant prototype using Takagi Sugeno fuzzy approach. International journal of hydrogen energy 2017; 42: 575-581. DOI: https://doi.org/10.1016/j.ijhydene.2017.02.167.

Evaluating efficiency of renewable energy sources in planning micro-grids considering uncertainties

Vu Van Thang

Thainguyen University of Technology, Thainguyen City, Vietnam, thangvvhtd@tnut.edu.vn
ORCID: 0000-0002-4440-749X

Nguyen Hien Trung

Thainguyen University of Technology, Thainguyen City, Vietnam, nguyenhientrung@tnut.edu.vn
ORCID: 0000-0001-8329-7097

Abstract: Nowadays, the renewable energy sources (RES) are widely utilized in micro-grids due to technical development and emission increase, which make the planning the micro-grids integrated the RES very important. To obtain the optimal planning strategy and evaluating efficiency of the RES in micro-grids, a mixed integer programming (MIP) planning framework for a grid-connected micro-grid is presented in this study. The understudy micro-grid consists of the wind turbines and photovoltaic systems, which are connected to utility grid through the point of common coupling (PCC). The objective function is minimizing the life cycle cost of object comprising of the investment and operation cost of the RES, the energy purchased cost from the utility grid, the emission taxes cost and the replacement cost or residual value of equipment at the end of the planning period. The uncertainties of load, electrical price, wind speed and solar radiation are taken into consideration and then a combinable model with the clustering technique is utilized to integrate them. Finally, numerical simulations for a test grid-connected micro-grid are made to validate the effectiveness of the proposed model and show efficiency of the RES to can apply to practical micro-grids.

Keywords: *Emission, Life cycle cost, Micro-grids planning, Renewable energy sources, Uncertainties*

1. INTRODUCTION

In recent decades, the demand in electricity increased while awareness of environmental protection increased as well, ensuing in a pledge to cut high emissions of traditional resources. Therefore, renewable energy sources are widely used as a result of this trend. They are connected to the low and medium voltage distribution system and create a new structure called micro-grid [1],[2]. A micro-grid can be designed to operate in either grid-connected or standalone mode. In grid-connected mode, the load can be supplied from both the renewable energy sources and diesel generators as well as from the utility grid through the point of common coupling (PCC) [[3],[4]]. The main benefit of this micro-grid mode is that it can still operate in a standalone mode when the connection to the utility grid is interrupted. The reliability of micro-grids is improved though the renewable sources cannot guarantee to supply power for the all of the load. Therefore, micro-grids are very promising to obtain an optimal planning strategy, evaluate efficiency of the RES and develop a green and sustainable energy system.

Many techniques of the RES have been researched, developed and applied in practice as photovoltaic panels, wind turbines, biogas-based internal combustion generators and micro-hydro generators with power less than 5MW [[5],[6]]. In recent years, the most popular renewable energy techniques have been the wind turbines (WT) and photovoltaic systems (PV) because they have the large potential, lower emissions and levelised cost of electricity than fossil fuel options [8]. Moreover, the various advantages when the RES integrated in optimal planning the micro-grids and distributed systems include the cost decrease, improved energy efficiency and higher resiliency, increased reliability, reduction in transmission losses and upgraded feeder deferment, emission reduction and a more flexible operation [9]-[11].

Because of all those reasons, numerous studies for planning, designing and operating of micro-grids considering the RES have been introduced in recent years [7,[12]. The optimal planning of isolated micro-grids with renewable energy resources handled through demand response or controllable loads is introduced in studies [13]. Their objective function includes the annual average cost of the initial investment, the cost replacement, operation, maintenance and demand response compensation or salvage value and power shortage penalty. Energy storage systems like the battery or pumped storage are utilized to guarantee supplying energy for any load, even when the output power of the RES is intermitted. In study [14], the grid-connected micro-grids planning process is presented with the objective to minimalize the total cost of planning project comprising of the investment and operation cost. All of them are the present-worth values because of discount rate in objective function. Similarly, a generation-side power scheduling and economic dispatch of distributed generators to grid-connected micro-grid is also represented in study [15]. The objective is to minimize operation costs that the user must pay for such as energy provided by the sources. The analyzed parameters of the micro-grid are assumed as unchanged values in these studies, despite of that they may be natural intermittent and are uncertain parameters, thus the error of the calculation result is often high.

To overcome those disadvantages, the uncertainties of the wind speed, natural gas price and annual load are represented by three values corresponding to probability of them. They are examined in an optimal model to design and operate a grid-connected micro-grid with objective function to minimize the overall cost of the electrical power, the fuel and incentive based demand response program [16]. However, the small state number and the ignored investment cost of distributed energy resources are limitations of this study. The planning models considering stochastic characteristic are introduced in study [17]. The objective function includes the equivalent annual value of investment cost, annual maintenance cost, fuel cost and environmental cost. Besides, the energy loss cost, energy not supplies cost and improving total voltage profile index are added in model of study [18]. Although these models do examine of equipment investment cost, the difference of lifetime and uptime of them is ignored in this study. The planning frameworks considering the uncertain parameters, lifetime of equipment and planning period

are presented in studies [20]-[22] with components of objective function that are the capital cost, operation and maintenance cost, replacement and salvage costs of the equipment at the end of the project. The unserved energy and reliability constraints are also considered to improve economic effectiveness and reliability of micro-grids. In addition, for a short planning period of micro-grid, the optimization method with an objective function based on minimal life cycle cost (LCC) is introduced in studies [23],[24] which aims to improve the effectiveness of the micro-grid planning problem. In these models, the LCC optimization theory is applied to take into consideration the cost during the entire duration of the project including the capital investment, the operation and maintenance cost, the recycling profit of scrapped equipment, the pollutant emission compensation cost and the energy shortage compensation cost. Those parameters of the simulation are unchanged values in this study, leading to a significant error of calculation result.

As described in detail above, the aspects of the micro-grid planning problem like uncertainty of parameters, investment and operation cost, replacement and salvage costs, lifetime of equipment and emission cost are studied and examined in optimal models. However, in each study, only several aspects are considered and that are the limitations of the present studies. Additionally, the decision variables utilized to select the power and capacity of the equipment are often continuous variables, despite being discrete values in fact. Because of those reasons, this study proposes a structure of grid-connected micro-grid, which can integrate and evaluate the efficiency of the RES in a scenario interested in the uncertainty of parameters. Then, an optimal model to plan the proposed micro-grid is created with a LCC objective function and constrains, which considers the uncertainty of the parameters as well as equipment lifetime and planning period of the project. The uncertainty of parameters is modeled by the probability density functions (pdf), the K-means clustering technique is utilized to divide into states and then a combinable model are applied to integrate in all states in the planning model. The binary variables are utilized in the model to select the rated sizes of equipment based on standard values and thus the results will be more accurate and the applicability of them in practice will be higher.

This study presents the modeling of those uncertainty parameters in Section 2, a detail description of the planning model in Section 3. The numerical simulations for computed cases are illustrated in Section 4 and the conclusions are given in Section 5.

2. STRUCTURE OF MICRO-GRID AND MODELING UNCERTAINTY OF PARAMETERS

2.1. Structure of micro-grid

To evaluate the efficiency of the RES in planning micro-grids, a grid-connected micro-grid with a structure shown in figure 1 is proposed. The demand of the load is supplied from the utility grid through PCC and RES. The PV and WT are chosen to examine further because of their great potential and it is easy to connect to the micro-grid. This structure has high reliability, the output power of the RES is not limited and thus the effectiveness of the RES is improved.
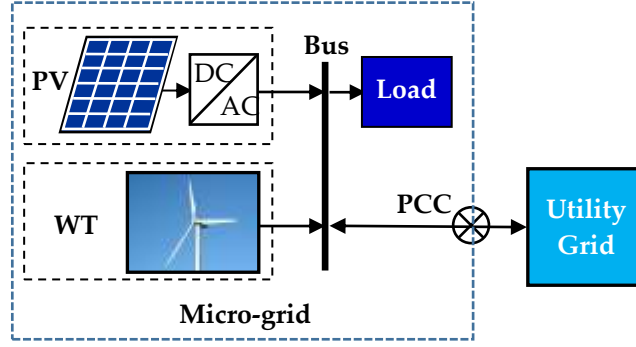
Figure 1. Structure of grid-connected micro-grid

2.2. Modeling uncertainty of parameters

As can be seen from figure 1, the uncertain parameters of the proposed micro-grid are the output power of the PV and WT, load and electrical price. The random change of them is modeled by the pdf and then the clustering technique is utilized to divide stochastic parameters into different states with specific values and their related probability in each state [23]-[27].

The randomness of solar irradiate is modeled by the beta distribution as in equation (1). I_{ir} is the solar irradiate at each state, μ is the mean and σ is the standard deviation of the stochastic variable [[18],[20],[28]]. In each state, the output power of the PV is calculated under the rated power P_r^{PV} at the standard test condition, solar irradiate and the operating ambient temperature as (2). In which, the standard test condition means that solar irradiate $I_{ir.stc}$ is 1000 W/m² and temperature T_{stc} is 25⁰C, $I_{ir.s}$ is the irradiate and $T_{c.s}$ is temperature of PV at operating state, and k_T is the power temperature coefficient of the PV.

$$f_b(I_{ir}) = \begin{cases} \dfrac{\Gamma(\alpha+\beta)}{\Gamma(\alpha).\Gamma(\beta)}.I_{ir}^{(\alpha-1)}.(1-I_{ir})^{(\beta-1)} & if\ 0 \le I_{ir} \le 1 \\ 0 & else \end{cases}$$

$$\beta = (1-\mu).\left(\frac{\mu.(1+\mu)}{\sigma^2}-1\right); \quad \alpha = \frac{\mu.\beta}{1-\mu} \tag{1}$$

$$P_s^{PV}(I_{ir}) = P_r^{PV}.\frac{I_{ir.s}}{I_{ir.stc}}.\left[1+k_T\left(T_{c.s}-T_{stc}\right)\right] \tag{2}$$

Similarly, the stochastic behavior of wind speed v is modeled by weibull distribution shown in expression (3) with the shape index k and the scale index c [[18],[20],[28]]. In each state s of wind speed, the output power of the WT is determined in equation (4) with output power P_s^{WT}, rated power P_r^{WT}, cut-in speed v_{ci}, rated speed v_{cr}, and cut-off speed v_{co} of WT.

$$f_r(v) = \frac{k}{c}\left(\frac{v}{c}\right)^{k-1}.\exp\left(-\left(\frac{v}{c}\right)^{k-1}\right); \quad c = \frac{\mu}{\Gamma\left(1+\dfrac{1}{k}\right)}; \quad k = \left(\frac{\sigma}{\mu}\right)^{-1.086} \tag{3}$$

$$P_s^{WT}(v) = \begin{cases} 0 & v_s \le v_{ci} \text{ or } v_{co} \le v_s \\ P_r^{WT} \cdot \dfrac{v_s - v_{ci}}{v_r - v_{ci}} & v_{ci} \le v_s \le v_r \\ P_r^{WT} & v_r \le v_s \le v_{co} \end{cases} \qquad (4)$$

The normal distribution is utilized to model the stochastic change of the load as present in equation (5) , where x is the load power, μ is the mean of the distribution, σ is the standard deviation and σ^2 is variance of the load at each state s [[17],[18]]. Analogously, the electricity price of the competitive market is also a stochastic parameter and expressed by the normal distribution in equation (5)[[29],[31]] with x for the value of the electrical price at state s.

$$f(x) = \frac{1}{\sigma\sqrt{2\pi}} \exp\left[-\frac{(x-\mu)^2}{2\sigma^2} \right] \qquad (5)$$

The multi-state parameters of the micro-grid as the output power of the PV and WT, load and electrical price are integrated by a combinable model introduced in studies [[31],[31]]. A matrix is utilized to enumerate all combination of states of parameters as equation (6) with C_s as the matrix enumeration the possible values of parameters. $\lambda_s\{C_s\}$ is a one-column matrix representing probability corresponding with the matrix C_s and N_s, which is the sum of individual states of the matrix M, is computed by product the possible states of the parameters.

$$\begin{aligned} M &= \{C_s, \ \lambda_s\{C_s\}\} \\ \lambda_s\{C_s\} &= \lambda_s^\rho\{\rho_s\} . \lambda_s^L\{P_s^L\} . \lambda_s^{WT}\{P_s^{WT}\} . \lambda_s^{PV}\{P_s^{PV}\} \\ N_s &= n_s^\rho . n_s^L . n_s^{WT} . n_s^{PV} \\ &\forall s \in N_s \end{aligned} \qquad (6)$$

Where, ρ_s and P_s^L are the electricity price and load corresponding with probabilities λ_s^ρ and λ_s^L, respectively. The P_s^{WT}, P_s^{PV} are the output power of WT and PV corresponding with probabilities λ_s^{WT} and λ_s^{PV}, respectively. The n_s^λ, n_s^L are the numbers of states assumed of the electricity price and load while the n_s^{WT}, n_s^{PV} that are the numbers of states of the output power of RS, respectively.

The numbers of scenarios to calculate N_S are very big depending on the chosen number of states in each pdf. Choosing the number of states is very important because of its effect on the accuracy of results and the complexity of the calculation. When numberous of scenarios selected, the accuracy is higher but computational burdens increase and vice versa.

3. MATHEMATICS MODEL

An optimal model is introduced with the LCC objective function including the investment cost, replacement cost or residual value of the RES at the end of planning period, operation and maintenance cost, and reduced emission cost of micro-grid during time the project. The micro-grid operation cost includes that of the RES plus the cost of energy purchase from the utility grid with the market price at the PCC. The reduced emission cost of micro-grids is calculated based on the difference in emissions between traditional energy sources and the RES. The objective function is evaluated in terms of

discounted costs, where discount rates are incorporated in the present-worth cost components as presented in equation (7).

$$Min\sum_{t=1}^{T}\frac{1}{(1+r)^t}\left(C_{I.t}^R + C_{OM.t}^R + C_{E.t}^G - B_{Emi.t} - B_{Res.t}\right) \qquad (7)$$

Where, the $C_{I.t}^R$ is the investment cost and $C_{OM.t}^R$ is the operation and maintenance of the RES. The $C_{E.t}^G$ is the cost for purchasing energy from the utility grid, the $B_{Emi.t}$ is the benefit or reduced cost due to decrease of emission taxes of the RES. $B_{Res.t}$ is the residual value or replacement cost of the RES at the end of the project, r is discount rate and T is the total planning time.

The investment cost of the RES is analyzed in equation (8) with capital cost C_k^R and invested power $P_{I.k,t}^R$ of the RES technology k at the year t that depends on rated powers, which is discrete values and the binary variable $\alpha_{i.k}$ in constraint (15). N_k is total number of RES technologies considered for investment.

$$C_{I.t}^R = \sum_{k=1}^{N_K} C_k^R . P_{I.k,t}^R \qquad \forall t \in T \qquad (8)$$

The operation and maintenance cost of the RES is analyzed based on average cost of an electrical energy unit that the RES generate in equation (9). Where, $\rho_{OM.k}^R$ is the coefficient for determining the operation and maintenance cost, $P_{k,t}^R$ is the power of the RES with type k at the year t, λ_s is probability in state s, and $k_{k,s}^R$ is the output power factor of the RES type k in state s. Similarly, the cost of electrical energy purchased from the utility grid depends on the power received through PCC $P_{t,s}^G$ in state s in equation (10) with the electrical energy price ρ_E^G and the annual rise factor of it k_ρ.

$$C_{OM.t}^R = 8760\sum_{k=1}^{N_K}\sum_{s=1}^{N_S}\rho_{OM.k}^R . \lambda_s . k_{k,s}^R . P_{k,t}^R \qquad \forall t \in T$$

$$P_{k,t}^R = P_{k,t-1}^R + P_{I.k,t}^R \qquad \forall t \in T \qquad (9)$$

$$C_{E.t}^G = \sum_{s=1}^{N_S} k_\rho . \rho_E^G . \lambda_s . P_{t,s}^G \qquad \forall t \in T \qquad (10)$$

The emission of the RES is lower than the traditional energy sources and thus the emission of micro-grids reduces when the RES are invested and the cost for emission taxes diminishes. The benefit due to decrease of the emission taxes very year is computed by equation (11). Where, ξ_G and ξ_{RS} are CO_2 emission coefficients of traditional sources and the RES, respectively, and β is the emission tax probably enforced by the government.

$$B_{Emi.t} = \beta.(\xi_G - \xi_{RS}).8760.\sum_{k=1}^{N_K}\sum_{s=1}^{N_S}\lambda_s . k_{k,s}^R . P_{k,t}^R \qquad \forall t \in T \qquad (11)$$

Analyzing the replacement cost or residual value of the RES at the end of the planning period is computed by expression (12) with the lifetime, $T_{c.k}^R$, the installed time $t_{I.k}^R$ and the uptime $t_{up.k}^R$. At the end of the analyzing time, if the uptime of the RES is shorter than the lifetime of them, $B_{Res.t}$ is the residual value and it becomes the replacement cost on the contrary.

$$B_{Res.t} = \frac{T_{c.k}^R - t_{up.k}^R}{T_{c.k}^R} C_{I.t}^R \quad \forall t \in T, k \in N_K$$

$$t_{up.k}^R = T - t_{I.k}^R \qquad \forall k \in N_K$$

(12)

The power balance constraint of the micro-grid in each state s as represented in equation (13) consist of the purchased power from the utility grid $P_{t,s}^G$, the output power of the RES and the load power. Where, the k_s^L is the load factor at each state s and P_t^L is load power at the year t determined in equation (14). P_0^L is the load value at base year and k_g^L is annual growth factor of the load.

$$P_{t,s}^G + \sum_{k=1}^{N_K} k_{k,s}^R . P_{k,t}^R = k_s^L . P_t^L \qquad \forall t \in T, s \in N_S$$

(13)

$$P_t^L = P_{t-1}^L .(1 + k_g^L) \qquad \forall t \in T$$

(14)

In fact, the RES are manufactured in modules with different rate powers, which are discrete values. Therefore, the integer variables $\alpha_{i.k}$ are utilized in constrain (15) to select the optimal number, rated power and of module types of the RES with the rated power of each technology k and module $P_{r.k,i}^R$. The power of the RES that can be harvested depends on the potential of the primary energy source in the micro-grid and thus the total power limit of each technology is constrained by equation (17) with $P_{k.max}^R$ that is limit power of each technology k.

$$P_{I.k,t}^R = \alpha_{k,i} P_{r.k,i}^R \qquad \forall t \in T, k \in N_K$$

(15)

$$\sum_{t=1}^{T} P_{I.k,t}^R \le P_{k.max}^R \qquad \forall k \in N_K$$

(16)

The maximum penetration of the RES in the micro-grid is limited based on the load power with the factor *x* in equation (17). This constraint guarantees that the power flow is always from the utility grid to micro-grid and thus the protection relay system is simpler. The power and energy that a micro-grid can be received from utility grid is assumed to be unlimited, because the power of the utility grid is much larger than power of micro-grids. However, the constraint (18) guarantees the equipment of the PCC not to be overload with S_{max}^{PCC} as maximum capacity.

$$\sum_{t=1}^{T} \sum_{k=1}^{N_K} P_{I.k,t}^R \le x.P_t^L$$

(17)

$$P_{t,s}^G \leq S_{max}^{PCC} \qquad \forall t \in T, s \in N_S \qquad (18)$$

The defined problem is a MIP model and is simulated for test micro-grid using GAMS/CPLEX software as below.

4. RESULTS and DISCUSSIONS

4.1. The parameters of test micro-grid

The test micro-grid has a structure as seen in figure 1. It is simulated with a load of 850 kW in base year and grows 5% annually. The rated power and module type of the PV and WT are discrete values and are assumed in table 1 [[32]-[36]]. Analogously, the parameters of the utility grid are also presented in table 1 with an CO_2 emission tax probably enforced by the government of 0.4cent/kg [[38],[38]]. The simulation period is 10 years and the discount rate is 10%.

The stochastic data of the load, output power of the PV and WT, and the electrical price are assumed and expressed by the pdf. Then K-means clustering technique is applied to divide into discrete values corresponding to each state s as shown in table 2 [[40],[40]]. The combinable model introduced in section 2 allows integration of all states and makes 11^4 (14641) scenarios [[26],[27],[29]].

Table 1. Parameters of the RES and the utility grid

PV		WT		Utility grid	
Rated power, $P_{r.k,i}^R$	50; 100; 120; 150; 200; 250; 300; 350; 430; 500 kW	Rated power, $P_{r.k,i}^R$	100; 120; 150; 195; 225; 255; 360; 420; 480; 510 kW	Limited capacity, S_{max}^{PCC}	1000 kVA
Capital cost, C_k^R	1500 \$/kW	Capital cost, C_k^R	1800 \$/kW	Electrical price, ρ_k^G	0.15 \$/kWh
O&M cost, $\rho_{OM.k}^R$	0.025 \$/kWh	O&M cost, $\rho_{OM.k}^R$	0.035 \$/kWh	Rise factor of price, k_ρ	1 %
Emission coefficient, ξ_R	0.025 kg/kWh	Emission coefficient, ξ_R	0.02 kg/kWh	Emission coefficient, ξ_G	0.62 kg/kWh
Lifetime, $T_{c.k}^R$	30 year	Lifetime, $T_{c.k}^R$	25 year		

4.2. Calculated results

The feasibility of the planning model and the efficiency of the RES in grid-connected micro-grid are investigated in two cases: In the first one, the micro-grid only purchases power from the utility gird (called without RES) and in the second one, the RES are additionally invested in the micro-grid to compare with the first case (called with RES).

Table 3 presents the invested decision of the RES in planning period with the number, rated power and type of modules, and installed time. Two PV modules with rated power of 250kW are selected to invest. They have a total rated power installed 500kW in the seventh year. Hence, the electrical energy purchased from the utility grid reduces 29.41% as shown in figure 2. Similarly, the only one module of WT has a rated power of 510kW and is implemented during time of project and it is installed at the eighth year. Total rated power of the RES is 1010kW corresponding to 84.45% of peak load of the micro-grid at eighth year.

Table 2. Probability of parameters

State	PV		WT		Load		Electrical price	
	k_s^{RS}	λ_s^{PV}	k_s^{RS}	λ_s^{WT}	k_s^L	λ_s^L	k_s^ρ	λ_s^ρ
1	1	0.014	1	0.007	1	0.01	1	0.028
2	0.9	0.024	0.95	0.025	0.85	0.056	0.90	0.043
3	0.8	0.069	0.85	0.032	0.77	0.106	0.80	0.085
4	0.7	0.087	0.75	0.045	0.71	0.165	0.75	0.096
5	0.6	0.081	0.65	0.051	0.65	0.165	0.70	0.129
6	0.5	0.073	0.55	0.077	0.59	0.163	0.65	0.142
7	0.4	0.052	0.45	0.091	0.51	0.163	0.60	0.137
8	0.3	0.045	0.35	0.112	0.45	0.091	0.55	0.126
9	0.2	0.031	0.20	0.103	0.41	0.047	0.50	0.102
10	0.1	0.028	0.15	0.101	0.35	0.034	0.45	0.081
11	0	0.497	0	0.354	0.30	0.00	0.40	0.031

Table 3. Invested decision of the RES

Types of the RES	Number of modules	Rated power of module, $P_{r.k,i}^R$ (kW)	Total power, $P_{I.k,t}^R$ (kW)	Planning year
PV	2	250	500	7
WT	1	510	510	8
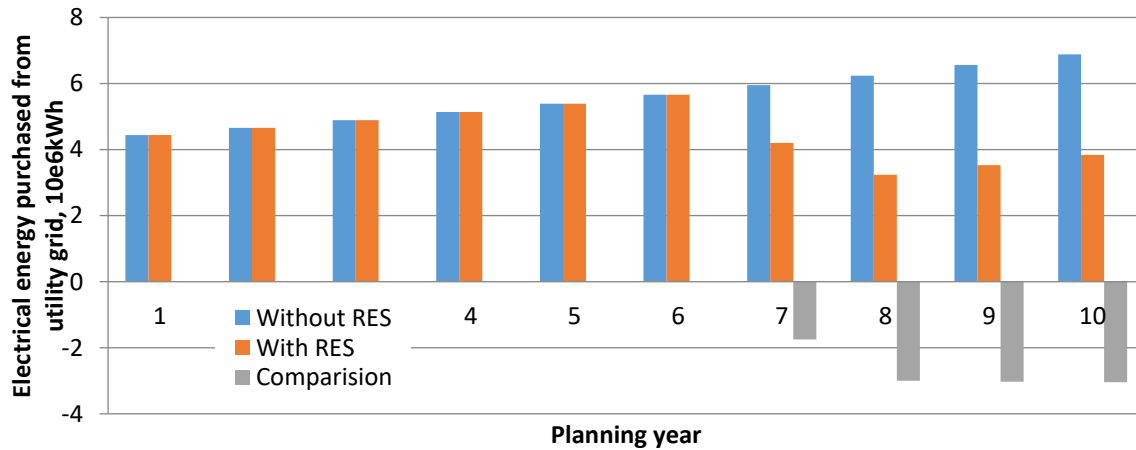
Figure. 2. Electrical energy purchased from the utility grid

When the RES are installed, the electrical energy purchased from the utility grid significantly reduces as shown in figure 2. In the case without RES, it is 4.44×10^6 kWh in the first year and increases to 6.88×10^6 kWh in the tenth planning year. However, the electrical energy received from utility grid decreases 1.75×10^6 kWh corresponding with 29.41% when two PV modules are installed in the seventh year. In the eighth year, one WT module is installed with a rated power 510kW and thus this reduction increases to 3.0×10^6 kWh each year corresponding with 48.08% in the eighth year, 46.19% in the ninth year and 44.19% in the tenth year.

Because of reasons above, the CO_2 emission decreases from 34.6×10^3 tons in the case without RES to 28.11×10^3 tons in the case with RES. Hence, it is decreased about 6.49×10^3 tons along with the emission tax that is reduced by 25.97×10^3\$ during the planning period as shown in table 4. In addition, the LCC of the project reduces about 0.22M\$ corresponding to 5.98% although the investment cost of the RES is high and equal 0.81M\$ at net present value.

Table 4. Comparison of economic and technical indicators of planning project in two cases

Economic and technical indicators	Without RES	With RES	Comparison between with RES case and without RES case
Total life cycle cost, M$	3.68	3.46	-0.22
Invested cost, M$	0	0.81	0.81
Total electrical energy purchased from utility grid, 10^6 kWh	55.81	44.99	-10.82
CO_2 emission, 10^3 tons	34.60	28.11	-6.49
Emission taxes cost, 10^3 $	138,41	112.44	-25.97

The results above show that the effect of the RES in micro-grid planning is significant in both economic and technical indicators due to a reduction of both the LCC and emission. Moreover, the reliability of the micro-grids is also improved because of some portion of power for loads are still supplied by the RES when the utility grid is faulty. The reduction of the power received from the utility grid through PCC also defers upgrading the connectible equipment.

5. CONCLUSIONS

In this research, a multi-scenario planning framework for grid-connected micro-grid is presented with an examination of investment in RES with respect to the uncertainty parameters based on minimizing the LCC of the invested project. The proposed model features a number of important aspects:

The multi-scenario planning framework proposed with the objective function and constraints can determine the optimal number, rated power and technology of modules as well as installed time of the RES. The objective function is minimizing the LCC during the time of the project that includes the investment cost, operation and maintenance cost of the RES, the electrical energy purchased cost from the utility grid, the emission taxes cost and the replacement cost or residual value of equipment at the end of the planning period. Hence, the different lifetime and the uptime of the RES are examined which improve the accuracy and suitability of model for the practical planning problem.

The uncertainties of parameters are considered and modeled by the pdf, the K-means clustering technique is utilized to divide into different states with specific value and the related probability in each state to reduce the computational burden. Then, a combinable model integrates all the states of parameters such as the electrical price, load and the output power of the PV and WT.

The proposed model utilizes integer variables to perform the invested decision of the RES based on rated power of different modules that are discrete values. Therefore, the computed result determines the number of modules with rated power and type of them, which agree with the actual parameters.

The simulation results demonstrate how the high efficiency of the RES in planning grid-connected micro-grid because the RES could promote the reduction of LCC and the cost for purchasing electrical energy from the utility grid. Particularly, the emission of the micro-grid significantly decreases and that has great significance in the context of climate change today.

The cases study has illustrated the feasibility and effectiveness of the proposed model, which indicates that the RES have high efficiency in reducing the cost and emission, and the optimization method could be brought into practice.

REFERENCES

[1] Prieto-Araujo, E, Olivella-Rosel, P, Cheah-Mañe, M, Villafafila-Robles, R, Gomis-Bellmunt, O. Renewable energy emulation concepts for microgrids. Renewable and Sustainable Energy Reviews 2015; 50: 325-345.

[2] Kaur, S, Kaur, T. A Review of Microgrid Concept. International Journal of Advanced Research in Science, Engineering and Technology 2016; 3: 1513-1520.

[3] Chen, D, Xu, L. AC and DC Microgrid with Distributed Energy Resources. In: Veneri, Ottorino. Technologies and Applications for Smart Charging of Electric and Plug-in Hybrid Vehicles. Cham, Switzerland: Springer International Publishing Switzerland, 2017. pp. 39-64.

[4] Ahmed, M, Amin, U, Aftab, S, Ahmed, Z. Integration of Renewable Energy Resources in Microgrid. Energy and Power Engineering 2015; 7: 12-29.

[5] Theo, WL, Limb, JS, Ho, WS, Hashim, H, Lee, CT. Review of distributed generation system planning and optimisation techniques: Comparison of numerical and mathematical modelling methods. Renewable and Sustainable Energy Reviews 2017; 67: 531-573.

[6] Sambaiah, KS. A Review on Optimal Allocation and Sizing Techniques for DG in Distribution Systems. International Journal of Renewable Energy Research 2018; 8: 1236-1256.

[7] Singh, B, Sharma, J. A review on distributed generation planning, Renewable and Sustainable Energy Reviews 2017; 76: 529-544.

[8] IRENA, International Renewable Energy Agency, Renewable Power Generation Costs 2017, Abu Dhabi, UAE, 2017.

[9] Kapoor, P, Singh, MKR, Shashikant. A Review on Distributed Generation Definitions and DG Impacts on Distribution System. International Journal of Innovative Science and Modern Engineering 2017; 4: 1-6.

[10] Latreche, Y, Bouchekara, HREH, Kerrour, F, Naidu, K, Mokhlis, H, Javaid, MS. Comprehensive review on the optimal integration of distributed generation in distribution systems. Journal of Renewable and Sustainable Energy 2018; 10: 1-33.

[11] Mumtaz and Bayram, IS. Planning, Operation, and Protection of Microgrids: An Overview. Energy Procedia 2017; 107: 94-100.

[12] Gamarraa, C. and Guerrero, JM. Computational optimization techniques applied to microgrids planning: a review. Renewable & Sustainable Energy Reviews 2015; 48: 413-424.

[13] Jing, Z, Zhu, J, Hu, R. Sizing optimization for island microgrid with pumped storage system considering demand response. J. Mod. Power Syst. Clean Energy 2018; 6: 791-801.

[14] Wang, Z, Chen, Y., Mei, S, Huang, S, Xu, Y. Optimal expansion planning of isolated microgrid with renewable energy resources and controllable loads. IET Renew. Power Gener. 2017; 11: 931-940.

[15] Lotfi, H, Khodaei, A. Co-Optimization Generation and Distribution Planning in Microgrids. In: IEEE International Conference on Smart Grid Communications; 23-26 October 2017: Germany, pp .1-6.

[16] Hernández, ACL, Aldana, NLD, Andrade, F, Graells, M, Guerrero, JM, Vasquez, JC. Economic Power Dispatch of Distributed Generators in a Grid-Connected Microgrid. In: ICPE-ECCE Asia. The 9th International Conference on Power Electronics and ECCE Asia; 1-5 June 2015: South Korea, pp. 1161-1168.

[17] Ahamdi, SP, Lordejani, SN ,Rahimi-Kian, A, Milasi, AM, Vahdati, PM. Uncertainty based configuration design and optimal operation of a grid-connected Micro-Grid. In: 2013 Smart Grid Conference (SGC), 17-18 December 2013: Iran, pp. 102-107.

[18] Fang, W, Liu, H, Chen, H, Zheng, H, Hua, G, He, W. DG planning in stand-alone microgrid considering stochastic characteristic. The Journal of Engineering 2017; 2017: 1181-1185.

[19] Gazijahani, FS, Salehi, J. Optimal Bi-level Model for Stochastic Risk-based Planning of Microgrids Under Uncertainty. IEEE Transactions on Industrial Informatics 2018; 14: 3054-3064.

[20] Khodaei, A, Bahramirad, S, Shahidehpour, M. Microgrid Planning Under Uncertainty. IEEE Transactions on Power Systems 2015; 30: 2417-2425.

[21] Jahangir, H, Ahmadian, A, Golkar, MA. Opyimal desigh of standalone micro-grid considering reliability and investment cost. In: CIRED Workshop; 14-15 June 2016: Helsinki, pp. 1-4.

[22] Nadimi, A, Adabi, F. Optimized Planning for Hybrid Microgrid in Grid-Connected Mode. International Journal of Renewable Energy Research 2016; 6: 494-503.

[23] Wand, C, Jiao, B, Guo, L, Yuan, K, Ssun, B. Optimal planning of stand-alone microgrids incorporating reliability. J. Mod. Power Syst. Clean Energy 2014; 2: 195-205.

[24] Liu, Z, Chen, Y, Luo, Y, Zhao, G, Jin, X. Optimized Planning of Power Source Capacity in Microgrid Considering Combinations of Energy Storage Devices. Appl. Sci. 2016; 6: 1-19.

[25] González, A, Riba, JR, Rius, A. Optimal Sizing of a Hybrid Grid-Connected Photovoltaic–Wind–Biomass Power System. Sustainability 2015; 7: 12787-12806.

[26] Jasemia, M, Adabi, F, Mozafari, B, Salahi, S. Optimal Operation of Micro-Grids Considering the Uncertainties of Demand and Renewable Energy Resources Generation. Int. Journal of Renewable Energy Development 2016; 5: 233-248.

[27] Atwa, YM, El-Saadany, EF. Probabilistic approach for optimal allocation of wind based distributed generation in distribution systems. IET Renew. Power Gener. 2011; 5: 79-88.

[28] Atwa, YM, El-Saadany, EF, Salama, MMA, Seethapathy, R. Optimal Renewable Resources Mix for Distribution System Energy Loss Minimization. IEEE Transactions on Power System 2010; 25: 360-370.

[29] Zhao, B, Zhang, X, Chen, J, Wang, C, Guo, L. Operation Optimization of Standalone Microgrids Considering Lifetime Characteristics of Battery Energy Storage System. IEEE Transactions on Sustainable Energy 2013; 4: 934-943.

[30] Soroudi, A, Mohammadi-Ivatloo, B, Rabiee, A. Energy Hub Management with Intermittent Wind Power. Large Scale Renewable Power Generation. In: J. Hossain and A. Mahmud. Large Scale Renewable Power Generation, Green Energy and Technology. Cham, Switzerland: Springer International Publishing Switzerland, 2014. pp. 413-438.

[31] Thang, VV, Zhang, Y, Ha, TT, Liu, S. Optimal operation of energy hub in competitive electricity market considering uncertainties. International Journal of Energy and Environmental Engineering 2018; 9: 351-362.

[32] Liu, Z, Wen, F, Ledwich, G. Optimal Siting and Sizing of Distributed Generators in Distribution Systems Considering Uncertainties. IEEE Transactions on Power Delivery 2011; 26: 2541-2551.

[33] Catalogue of European Urban Wind Turbine Manufacturers, Wind Energy Integration in the Urban Environment (WINEUR) 2018, http://www.urbanwind.net/wineur.html.

[34] IRENA, Renewable Power Generation Costs in 2017, International Renewable Energy Agency, Abu Dhabi, pp. 1-158.

[35] Sollatek Solar Catalogue 2018, https://www.sollatek.com/product-category/solar-products/.

[36] Bayod-Rújula, AA, Yuan, Y, Martínez-Gracia, A, Wang, J, Uche, J, Chen, H. Modelling and Simulation of a Building Energy Hub. Proceedings 2018; 2: 1-6.

[37] Amir, V, Jadid, S, Ehsan, M. Optimal Planning of a Multi-Carrier Microgrid Considering Demand-Side Management. International Journal of Renewable Energy Research 2018; 8: 238-249.

[38] Gong, Q, Lei, J, Ye, J. Optimal Siting and Sizing of Distributed Generators in Distribution Systems Considering Cost of Operation Risk. Energies 2016; 9: 1-18.

[39] Deng, S, Wu, Q, Jing, Z, Wu, L, Wei, F, Zhou, X. Optimal Capacity Configuration for Energy Hubs Considering Part-Load Characteristics of Generation Units. Energies 2017; 10: 2-19.

[40] Chen, Z, Yan, Z. Scenario tree reduction methods through clustering nodes. Computers and Chemical Engineering 2018; 109: 96-111.

[41] Xu, D, Chen, Z, Yang, L. Scenario tree generation approaches using K-means and LP moment matching methods. Journal of Computational and Applied Mathematics 2012; 236: 4561-4579.

Impacts of edge seal material on thermal insulation performance of a thermally resistive photovoltaic glazing: CFD research with experimental validation

Erdem Cuce

Recep Tayyip Erdogan University, Faculty of Engineering, Department of Mechanical Engineering, Rize, Turkey

Recep Tayyip Erdogan University, Faculty of Engineering, Low/Zero Carbon Energy Technologies Laboratory, Rize, Turkey

erdem.cuce@erdogan.edu.tr

ORCID:0000-0003-0150-4705

Abstract: A novel design of photovoltaic (PV) glazing technology called TRPVG is introduced within the scope of this research, and thermal insulation performance of TRPVG for different edge seal materials is evaluated through a well-known and reliable commercial software ANSYS FLUENT. For a typical TRPVG configuration, CFD results are compared with the experimental data, and a good accordance is achieved. Then, different potential edge seal materials are considered for TRPVG technology in terms of their impacts on thermal bridging and hence overall heat transfer coefficient (U-value) of entire glazing. Besides the plastic based edge seals, which are widely utilized in fenestration products, thermal superinsulation materials like flexible aerogel are also considered in the research to analyze their potential effects for reducing the U-value range of TRPVG. A recent experimental research indicates a U-value of 1.10 W/m2K in which unplasticised polyvinyl chloride (PVC-U) is considered as edge seal. The U-value from the CFD research for the said configuration is determined to be 1.19 W/m2K, which verifies the accuracy of the numerical analyses. Further investigations reveal that the U-value of TRPVG can be enhanced to 1.13 W/m2K only if PVC-U edge seal is replaced with aerogel. This can be attributed to the competitively low thermal conductivity of PVC-U material (0.19 W/mK) as an edge seal. The predicted U-values of TRPVG are reported to be 1.44 W/m2K for polymer seal, 1.32 W/m2K for glass fiber seal, 1.26 W/m2K for polycarbonate seal, 1.24 W/m2K for polyethylene seal, 1.20 W/m2K for acrylic seal and 1.18 W/m2K for epoxy seal.

Keywords: *PV glazing, U-value, Edge seal material, Thermal insulation, CFD*

1. INTRODUCTION

Buildings are responsible for about 40% of total energy consumed worldwide. In this sense, building sector is considered as one the most sensitive fields for urgent mitigation of total world energy consumption figures in most of the developed and developing countries [1]. The dramatic role of buildings in global energy use can be ascribed to the insufficient thermal insulation features of existing building elements [2] as well as poor electrical and thermal efficiency ranges of conventional energy systems utilized in buildings [3]. As a consequence of this, there is a noticeable stimulation into alternative thermally resistive building materials [4] along with the energy-efficient, cost-effective and eco-friendly energy technologies toward low/zero carbon building standards [5]. Moreover, bioinspired strategies are evaluated for potential retrofit applications in buildings [6].

When a typical building envelope is taken into consideration, the poorest building element in terms of thermal insulation performance is identified as windows [7]. Approximately 60% of heat losses from building fabric are attributed to glazed areas. In this respect, a significant number of glazing technologies is in the center of interest to be able to meet the low/zero carbon performance figures proposed in latest building codes [8]. Among the all types of window technologies, PV glazing technology draws a remarkable attention of researchers especially within the last two decades owing to its multifunctional features. A typical PV glazing is capable of generating electricity when the external surface of the unit is subjected to sunlight [9]. PV glazing is widely preferred in modern architecture because of aesthetic aspects. It can be considered as an entire building element through building integrated PV and PV/Thermal (BIPV and BIPVT) applications. Especially BIPVT air collectors have a great potential to lead the fenestration market in the near future when optimum tilt angle is considered [10] and passive cooling strategies are utilized in the system [11]. Despite all of the said advantages of PV glazing technology, it has some shortcomings as well regarding thermal insulation performance, which is of vital importance in terms of overall performance merit of a glazing product. This handicap is considered as the most significant challenge for the commercialization process of the PV glazing technology [12]. The U-value of PV glazing products is not promising when compared to the multilayer glazing technology, which is dominant in market. Therefore, recent attempts are usually made for improving poor U-value range of PV glazing products through cost-effective and eco-friendly modifications.

Sun et al. [13] consider semi-transparent cadmium telluride (CdTe) in PV glazing concept, and evaluate the daylighting and energy performance of the product for different configurations. The maximum electrical efficiency of CdTe PV glazing is reported to be about 22%. The average U-value of the product is determined to be 2.54 W/m^2K, which is competitive with air filled double glazed window. About 73% reduction in energy losses is achieved from the CdTe PV glazing as well as better daylighting performance in comparison with ordinary glazing. Cuce et al. [14] develop a novel design of PV glazing entitled heat insulation solar glass (HISG), and carry out several experimental studies on thermal insulation performance of the HISG unit. Semi-transparent amorphous silicon (a-Si) PV cells are utilized in the HISG unit with an electrical efficiency of about 9%. Owing to the highly thermally resistive layers behind the PV cells, an overall U-value of 1.10 W/m^2K is achieved from the HISG product. Energy generation performance of HISG is evaluated in another research conducted by Cuce et al. for actual operating conditions and under solar simulator [15]. The results reveal that HISG can generate more than 40 W electrical power for a solar intensity of 850 W/m^2 and for a PV glazing area of 0.66 m^2. Lighting and energy saving performance of HISG are also investigated, and it is found that this novel PV glazing technology is capable of blocking 100% of UV light. In addition, enhanced indoor conditions are obtained by preventing the glare effects [16].

Ghosh et al. [17] propose a new design of PV glazing by incorporating the vacuum concept into the unit as a superior thermal resistance layer. Their experimental results demonstrate that a promising U-value (0.80 W/m^2K) can be achieved from the said design, which is sufficient to meet the latest low/zero

carbon building standards. In comparison with the reference case of PV double glazing, 66% greater thermal resistance is obtained from the novel design. However, it needs to be noted that the said U-value is expected to deteriorate for longer operation periods due to probable losses in vacuum level. A similar attempt is carried out by Zhang et al. [18] through their novel design entitled vacuum PV insulated glass unit. A similar U-value is reported in their research for an entire product thickness of about 21 mm. It is underlined that the novel PV glazing structure not only remarkably reduces the cooling loads of buildings but also provides comfortable indoor environments. Wang et al. [19] experimentally analyze the thermal insulation performances of two different PV glazing structure namely PV double skin facade and PV insulating glass unit. The experimental results show that the PV insulating glass unit has somewhat a lower U-value (2.28 W/m^{2}K) than PV double skin facade (2.54 W/m^{2}K). Zhang and Lu [20] conduct a simulation research to assess the overall thermal insulation performance of PV insulating glass unit under several climatic conditions. It is observed from the results that low-e integrated PV glazing shows better U-value (1.62 W/m^{2}K) than the conventional PV glazing product with clear glass (2.64 W/m^{2}K).

Through the literature survey on PV glazing technology and potential strategies to reduce the U-value of PV glazing products in market, it is understood that the greatest part of efforts is essentially based on improving the thermal resistance of entire structure through additional layers provided behind such as inert gas or vacuum [21]. However, thermo-physical properties of materials utilized in PV glazing structure is also of vital importance in terms of overall thermal insulation performance. Replacing conventional support pillars inside Pilkington Spacia vacuum glazing with translucent aerogel and enhancing the U-value of vacuum glazing from 1.20 to 0.67 W/m^{2}K is a good example of this [22]. Especially edge seals can play a dramatic role in thermal bridging effects, which can result in poorer thermal insulation performance figures than expected. The impacts of edge seal materials on the average U-value of a typical glazing product can be much more remarkable when the thermal resistance inside the glazing is incomparably greater than that of around edges [23]. A wide range of materials is utilized as edge seal material in glazing products such as acrylic, epoxy, PVC-U, low and high density polyethylene, glass fibre, polycarbonate, etc. However, there is no research conducted so far to analyze the said edge seal materials on the U-value of windows. Therefore, a CFD analysis is carried out within the scope of this research to evaluate the contributive effects of the said materials on thermal bridging for a case of novel PV glazing technology called TRPVG. For a reference case, CFD results are first compared with the experimental data, and following the accuracy justification, numerical research is repeated for the rest of the materials for the first time in literature.

2. METHODOLOGY

2.1. Features of TRPVG

TRPVG differs from the conventional PV glazing products in market in terms of several aspects such as very high thermal resistance which is competitive with argon filled triple glazed windows, self-cleaning feature owing to the TiO$_2$ nano coating on the a-Si PV cells, thermally comfortable indoor conditions as a consequence of low-e coating integrated thermally resistive glass which yields to 100% blockage of UV and IR parts of incoming sunlight. Different configurations of TRPVG concept are devised, fabricated and tested through a comprehensive experimental and numerical optimization procedure. The numerical research is based on a reference design from a previous PV glazing technology called HISG. The constructional details of the reference TRPVG design are illustrated in Figure 1. TRPVG-Ar16 concept uses 16 mm thick argon as inert gas between a-Si PV cells and low-e integrated thermally resistive window pane. Argon as an inert gas provides excellent thermal resistance throughout the PV glazing structure. Low-e integrated thermally resistive window pane has a thermal conductivity of 0.96 W/mK. Low-e coating is slightly more thermally conductive (1.20 W/mK), however, due to its

negligible thickness, its impact on total heat transfer rate is ignored. PVC-U is utilized as edge seal material in the fabrication of TRPVG-Ar16. Thermal conductivity of PVC-U is 0.19 W/mK, which is satisfactory for such PV glazing applications. The poorest element in the construction in terms of thermal resistance is the a-Si PV module (1.50 W/mK). TiO_2 nano coating on the a-Si PV module enables self-cleaning feature, which is of vital importance for the tall buildings like skyscrapers. The aforesaid coating also reduces the reflection losses which yields to notable enhancements in electrical efficiency of the unit. TRPVG-Ar16 concept has an entire thickness of 28 mm.
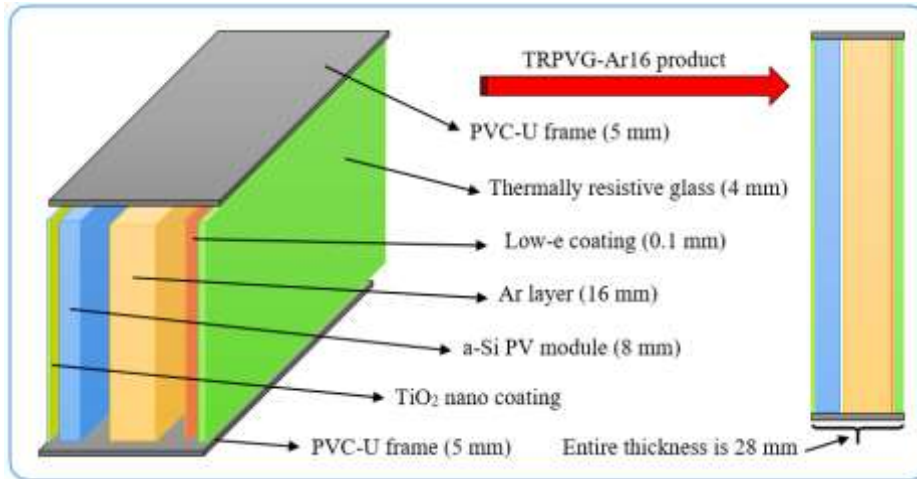
Figure 1. Constructional details of TRPVG-Ar16 product.

TRPVG-Ar16 is capable generating more than 100 W electrical power from per m^2 PV module area under standard test conditions (1000 W/m^2 solar intensity and 25 °C PV cell temperature). The production cost of TRPVG-Ar16 is slightly above 200 €/m^2, which is competitive with the market prize of conventional multilayer glazing products in Europe. The thorough thermo-physical properties of materials utilized in the fabrication of TRPVG-Ar16 is given in Table 1.

Table 1. Thermo-physical properties of materials inside TRPVG-Ar16

	d (kg/m^3)	c_p (J/kgK)	k (W/mK)
a-Si PV module	2330	703	1.50
Ar layer	1.6228	520.64	0.0158
Thermally resistive glass	2700	880	0.96
Low-e glass	2550	800	1.20
PVC-U	1400	900	0.19

In the fabrication of any type of PV glazing product, edge seal materials are utilized for thermal insulation and sealing purposes. Within the scope of the research project, several edge seal materials are considered from conventional to superinsulation material category. However, a reference product is also produced from PVC-U to justify the accuracy of the CFD analyses as experimental U-values on similar designs are available in literature.

2.2. CFD analysis

Within the scope of CFD analyses, a well-known, reliable and commercially available software ANSYS FLUENT is utilized. The geometry is constructed in GAMBIT which is in good accordance with the software. A 2D model is structured which is successful enough to simulate the heat transfer mechanisms within the PV glazing. TRPVG-Ar16 is subjected to natural convection internally and forced convection externally through internal and external surfaces, respectively. The indoor and outdoor temperatures and heat convection coefficients as well as thermo-physical properties of environmental chamber air considered in the CFD analyses are presented in Table 2. TRPVG-Ar16 is assumed to have adiabatic boundary conditions at the edges, however, heat transfer through the edge seal material is studied in the research, which is basically the goal of this work. By considering different edge seal materials, their

potential impacts on thermal bridging are numerically analyzed. PRESTO approach is preferred as a consequence of selecting pressure-based solver in the modelling of natural convection inside argon medium. Rectangular mesh is structured in the CFD analyses, and mesh-independent solution is achieved. Convergence criteria is selected to be 10^{-4} which is adequate for such a model. Convergence is easily secured by controlling the under-relaxation factors during the iteration process.

Table 2. Indoor and outdoor convection parameters utilized in CFD research

	d (kg/m^3)	c$_p$ (J/kgK)	k (W/mK)
Environmental chamber air	1.2250	1006.43	0.0242

	h (W/m^{2}K)	T (^{o}C)
Indoor air	5	25
Outdoor air	25	5

2.3. U-value analysis

The calculation of U-value for the TRPVG-Ar16 design is based on the numerical values produced by ANSYS FLUENT software. In this respect, total heat transfer rate across the PV glazing is determined through the reports section of the software. Then, through the surface integrals interface, area-weighted average surface temperatures are specified for both internal and external surfaces. Total heat transfer rate is divided by surface area of PV glazing and temperature difference between internal and external surfaces, which yields to the U-value of entire TRPVG-Ar16.

3. RESULTS and DISCUSSIONS

In this research, several potential edge seal materials are considered for TRPVG-Ar16 in terms of their effects on thermal bridging and thus the U-value of entire PV glazing. Prior to demonstrating the extended results, an accuracy justification is conducted through a reference case study in which PVC-U material is considered at the edges for sealing and thermal insulation purposes. For the thermo-physical properties of materials given in Table 1, and for the convection parameters listed in Table 2, contours of static temperature inside TRPVG-Ar16 are achieved as shown in Figure 2. It is understood from the data that the right hand side of the contour image is subjected to the indoor environment whereas the left hand side is exposed to outdoor conditions.
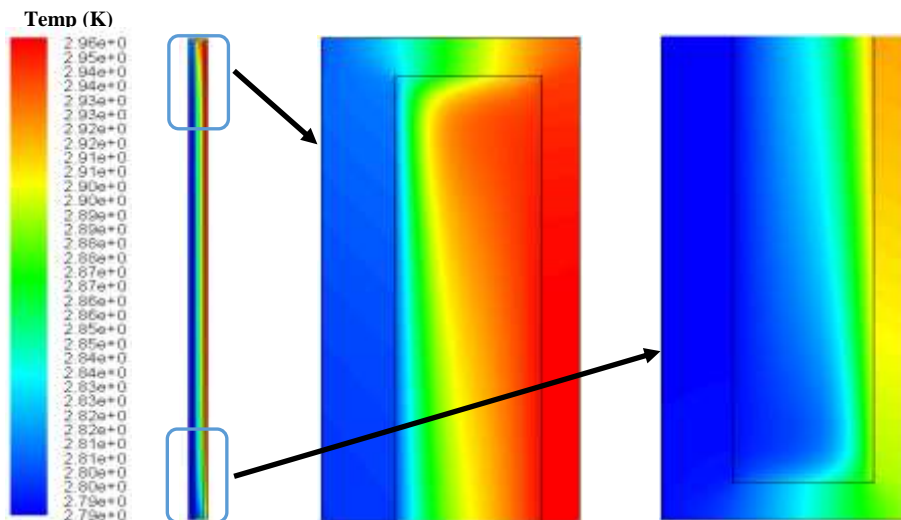
Figure 2. Contours of static temperature inside TRPVG-Ar16 and thermal behavior of the product.
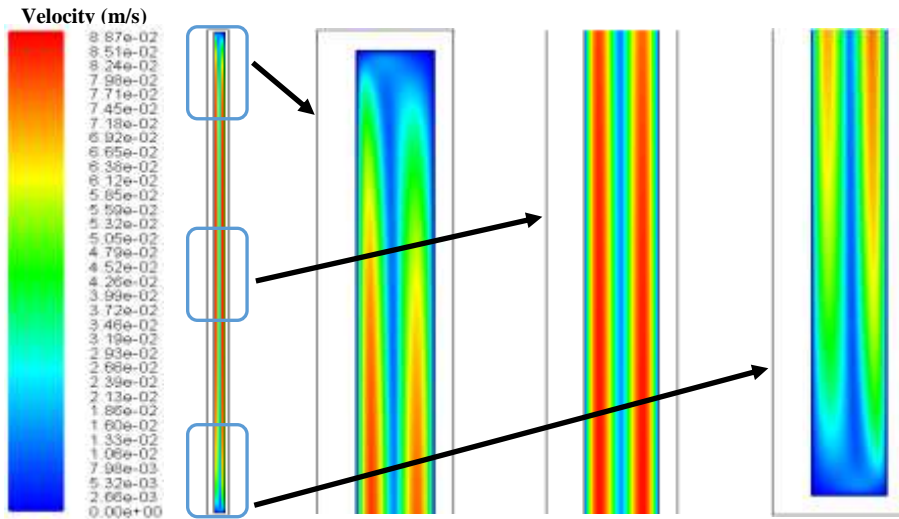
Velocity (m/s)

Figure 3. Contours of velocity magnitude inside TRPVG-Ar16.
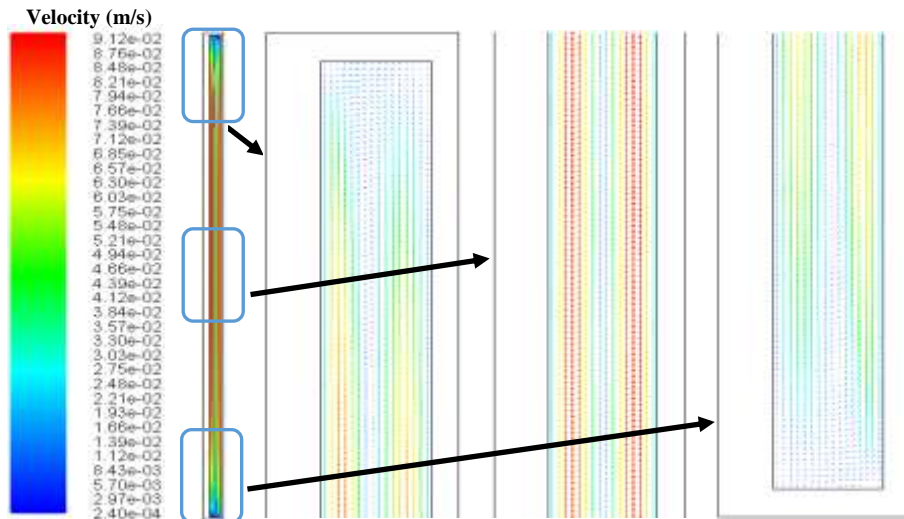
Velocity (m/s)

Figure 4. Natural convection effects and velocity vectors inside TRPVG-Ar16.

The contours of velocity magnitude inside TRPVG-Ar16 and the thermal behavior of the product are illustrated in Figure 3. It is observed from the data that noticeable natural convection effects take place within 16 mm thick argon medium as expected. However, owing to the somewhat high viscosity values of argon at room temperature, impacts of natural convection on total heat transfer rate across the product remain limited. Around central parts of TRPVG-Ar16, natural convection effects become maximum as predicted, and corresponding velocity value for the said parts are shown in Figure 4. The results indicate that the greatest velocity inside TRPVG-Ar16 is about 0.0912 m/s, which is reported around center. Natural convection effects are negligible around the edges which are covered with PVC-U material.

For the said boundary conditions, the total heat transfer rate from TRPVG-Ar16 is numerically determined to be 16.8873 W as shown in Figure 5. Following the determination of total heat transfer rate, the average temperatures of internal and external surfaces of TRPVG-Ar16 are specified as depicted in Figure 6.
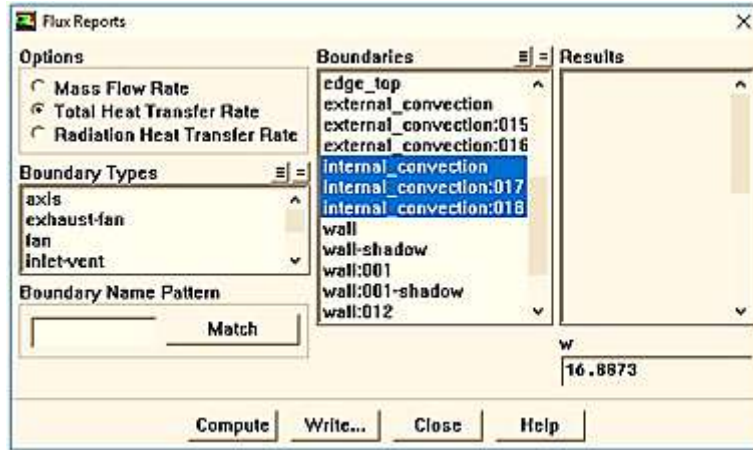
Figure 5. Total heat transfer rate across TRPVG-Ar16 product.
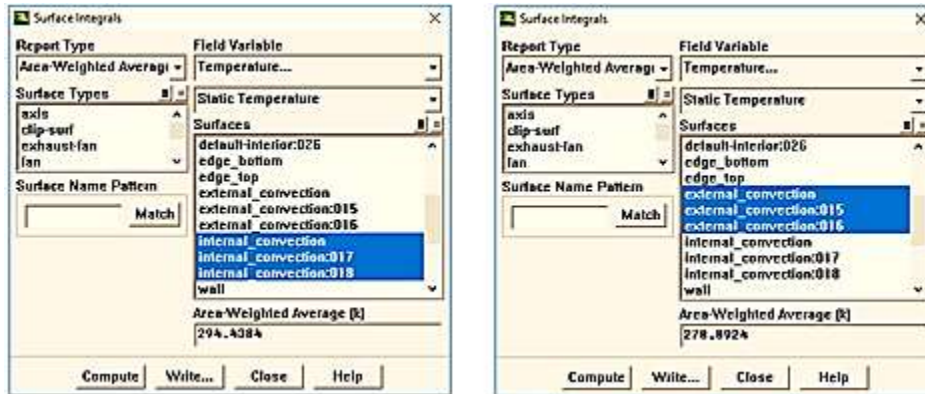
Figure 6. The average internal and external surface temperatures of TRPVG-Ar16 product.

The average internal surface temperature is determined to be 294.4384 K whereas it is 278.8924 K for the external surface. In other words, the temperature difference across TRPVG-Ar16 product is reported to be 15.5460 K. Total surface area of the product is 0.91 m². By a simple implementation of Newton's cooling law, the numerical U-value of TRPVG-Ar16 can be calculated as follows:

$$Q = UA\Delta T \qquad (1)$$

$$U = Q/A(T_{int} - T_{ext}) \qquad (2)$$

$$U = 16.8873/0.91(294.4384 - 278.8924) \qquad (3)$$

$$U = 1.19 \, W/m^2 K \qquad (4)$$

The numerical U-value from the CFD analysis (1.19 W/m²K) is compared with a reference product in recent literature called HISG which has similar configuration details. The experimental U-value of the reference product is reported to be 1.10 W/m²K [24], which is in good accordance with the numerical U-value achieved from the CFD research. The aforesaid experimental study is a typical application of

co-heating test procedure in literature [14]. In a typical co-heating test, the U-value of any building element is experimentally determined through hot box and environmental chamber test system. Hot box and environmental chamber represent the indoor and outdoor conditions in winter time, respectively. Hot box temperature is usually adjusted to 25 °C, while environmental chamber is set to 5 °C. Heat flow across the building element is measured by a sensitive heat flux sensor. In addition, internal and external surface temperature of the building element are determined via sensitive T or K type thermocouples. Through Newton's cooling law, U-value of the building element is specified. Co-heating test procedure is a well-known and reliable method in literature to investigate the thermal insulation performance of any type of building element.

Following the accuracy justification of the CFD analyses, different edge seal materials are investigated for novel TRPVG-Ar16 concept for the first time in literature in terms of their potential influences on the U-value of entire glazing. It is clear from the literature that plastic based edge seals are commonly utilized in fenestration products. Within the scope of this research, not only the said plastic type materials but also thermal superinsulation materials like flexible aerogel are considered for edge sealing, and the U-value range of TRPVG-Ar16 is numerically evaluated for each case.

The CFD analyses are repeated for different edge seal materials for the thermal conductivity range of 0.01-10 W/mK. The thermal conductivity of 0.01 W/mK [25] refers to the greatest thermal resistance at the edges which is provided by aerogel [26], whereas 10 W/mK corresponds to the poorest thermal resistance feature of polymer edge seal. The numerical U-values achieved from the CFD research are demonstrated in Figure 7.
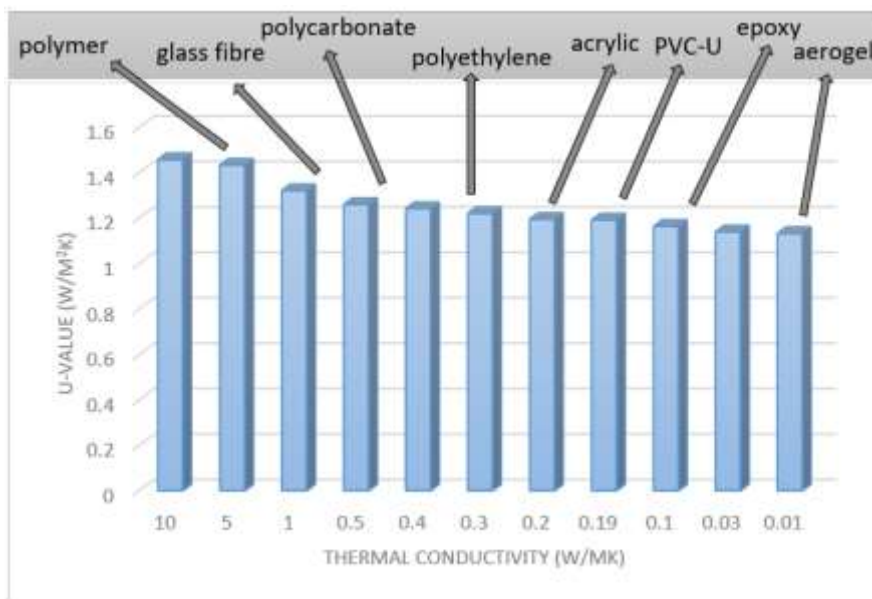
Figure 7. The U-value of TRPVG-Ar16 for different edge seal materials.

The estimated U-values of TRPVG-Ar16 are found to be 1.44 W/m^{2}K for polymer seal, 1.32 W/m^{2}K for glass fiber seal, 1.26 W/m^{2}K for polycarbonate seal, 1.24 W/m^{2}K for polyethylene seal, 1.20 W/m^{2}K for acrylic seal and 1.18 W/m^{2}K for epoxy seal. If aerogel as a thermal superinsulation material is considered at the edges, the overall U-value of TRPVG-Ar16 is only enhanced to 1.13 W/m^{2}K. Due to the remarkably higher unit cost of aerogel compared to the other potential edge seal materials, it is recommended to utilize epoxy or PVC-U in the entire design of novel TRPVG technology. Compared to the polymer seals, epoxy is determined to show 18% better thermal resistance, which is of vital importance to note.

4. CONCLUSION

PV glazing products in market are usually poor in terms of thermal insulation performance due to their remarkably high U-value ranges. A novel PV glazing technology called TRPVG-Ar16 is introduced, and its thermal insulation ability is numerically analyzed through a well-known and reliable commercial software ANSYS FLUENT. Edge seal materials' thermo-physical properties play a key role in overall heat transfer coefficient of PV glazing. Therefore, different edge seals are considered for TRPVG-Ar16, and the impacts of edge seal material on thermal bridging are numerically investigated. The results reveal that epoxy, PVC-U and acrylic show the best performance when thermal resistance and cost figures are taken into account at the same time. Polymer edge seals demonstrate the poorest thermal insulation feature as a consequence of their somewhat high thermal conductivity range. 18% lower U-value can be achieved from TRPVG-Ar16 if epoxy is utilized for edge sealing instead of polymer.

Acknowledgments

REFERENCES

[1] Cuce, E. Development of innovative window and fabric technologies for low-carbon buildings. Ph.D. Thesis, The University of Nottingham, Nottingham, United Kingdom, 2014.

[2] Volf M, Lupíšek A, Bureš M, Nováček J, Hejtmánek P, Tywoniak J. Application of building design strategies to create an environmentally friendly building envelope for nearly zero-energy buildings in the central European climate. Energy and Buildings 2018; 165: 35-46.

[3] Cuce PM, Cuce E. Toward cost-effective and energy-efficient heat recovery systems in buildings: Thermal performance monitoring. Energy 2017; 137: 487–494.

[4] Berardi U. Aerogel-enhanced systems for building energy retrofits: Insights from a case study. Energy and Buildings 2018; 159: 370-381.

[5] Cuce E, Cuce PM, Besir AB. Greenery systems toward low/zero carbon buildings. Chapter in Low Carbon Transition - Technical, Economic and Policy Assessment. London, United Kingdom, InTechOpen, 2018; 29-50.

[6] Cuce E, Nachan Z, Cuce PM, Sher F, Neighbour GB. Strategies for ideal indoor environments towards low/zero carbon buildings through a biomimetic approach. International Journal of Ambient Energy 2019; 40(1): 86-95.

[7] Cuce E. Accurate and reliable U-value assessment of argon-filled double glazed windows: A numerical and experimental investigation. Energy and Buildings 2018; 171: 100–106.

[8] Jelle BP, Hynd A, Gustavsen A, Arasteh D, Goudey H, Hart R. Fenestration of today and tomorrow: A state-of-the-art review and future research opportunities. Solar Energy Materials and Solar Cells 2012; 96: 1-28.

[9] Cuce E. Toward multi-functional PV glazing technologies in low/zero carbon buildings: Heat insulation solar glass - Latest developments and future prospects. Renewable and Sustainable Energy Reviews 2016; 60: 1286–1301.

[10] Cuce E, Cuce PM. Tilt angle optimization of building-integrated photovoltaics (BIPVs) for cooler operating temperatures. MEGS IV Annual Conference, Public Engagement with Energy. 12–13 September 2013, Loughborough, United Kingdom.

[11] Cuce PM, Cuce E. Passive cooling of building-integrated photovoltaics (BIPVs) for better electrical performance. MEGS IV Annual Conference, Public Engagement with Energy. 12–13 September 2013, Loughborough, United Kingdom.

[12] Cuce E. Recent developments on multi-functional PV glazing technologies: Heat insulation solar glass. Fifteenth International Conference on Sustainable Energy Technologies. 19-22 July 2016, Singapore.

[13] Sun Y, Shanks K, Baig H, Zhang W, Hao X, Li Y, He B, Wilson R, Liu H, Sundaram S, Zhang J. Integrated semi-transparent cadmium telluride photovoltaic glazing into windows: Energy and daylight performance for different architecture designs. Applied Energy 2018; 231: 972-984.

[14] Cuce E, Young CH, Riffat SB. Thermal performance investigation of heat insulation solar glass: A comparative experimental study. Energy and Buildings 2015; 86: 595–600.

[15] Cuce E, Young CH, Riffat SB. Performance investigation of heat insulation solar glass for low-carbon buildings. Energy Conversion and Management 2014; 88: 834–841.

[16] Cuce E, Young CH, Riffat SB. Thermal insulation, power generation, lighting and energy saving performance of heat insulation solar glass as a curtain wall application in Taiwan: A comparative experimental study. Energy Conversion and Management 2015; 96: 31–38.

[17] Ghosh A, Sundaram S, Mallick TK. Investigation of thermal and electrical performances of a combined semi-transparent PV-vacuum glazing. Applied energy 2018; 228: 1591-600.

[18] Zhang W, Lu L, Chen X. Performance evaluation of vacuum photovoltaic insulated glass unit. Energy Procedia 2017; 105: 322-326.

[19] Wang M, Peng J, Li N, Yang H, Wang C, Li X, Lu T. Comparison of energy performance between PV double skin facades and PV insulating glass units. Applied Energy 2017; 194: 148-160.

[20] Zhang W, Lu L. Overall energy assessment of semi-transparent photovoltaic insulated glass units for building integration under different climate conditions. Renewable Energy 2019; 134: 818-827.

[21] Cuce E, Cuce PM. Smart retrofit solutions of buildings toward a low carbon world. Energy Research Journal 2018; 9: 77-86.

[22] Cuce E, Riffat SB. Aerogel-assisted support pillars for thermal performance enhancement of vacuum glazing: a CFD research for a commercial product. Arabian Journal for Science and Engineering 2015; 40(8): 2233-2238.

[23] Lee W, Kang J, Cho SW. A New Structure of Vacuum Insulation Glazing for Edge Effect Reduction: A Parametric Study. International Journal of Precision Engineering and Manufacturing 2018; 19(3): 447-452.

[24] Cuce E, Cuce PM, Riffat SB. Novel glazing technologies to mitigate energy consumption in low-carbon buildings: A comparative experimental investigation. International Journal of Energy Research 2016; 40: 537–549.

[25] Cuce E, Cuce PM, Wood CJ, Riffat SB. Toward aerogel based thermal superinsulation in buildings: A comprehensive review. Renewable and Sustainable Energy Reviews 2014; 34: 273–299.

[26] Buratti C, Cuce E, Merli F, Moretti E. Thermal and acoustic properties of aerogels: Preliminary investigation of the influence of granule size. Eighth International Conference on Sustainability in Energy and Buildings. 11-13 September 2016, Turin, Italy.
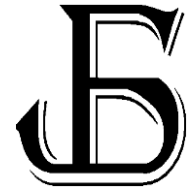
Design of an LLCL type filter for stand-alone PV systems' harmonics

Suleyman Adak

Mardin Artuklu University, Electrical and Energy Department, Mardin, Turkey, suleymanadak@yahoo.com, ORCID: 0000-0003-1436-2830

Hasan Cangi

Kahramanmaras Sutcu Imam University, Department of Electrical and Electronics Engineering, Kahramanmaras, Turkey, hasancangi@yahoo.com, ORCID: 0000-0001-6954-7299

Ahmet Serdar Yilmaz

Kahramanmaras Sutcu Imam University, Department of Electrical and Electronics Engineering, Kahramanmaras, Turkey, asyilmaz@ksu.edu.tr, ORCID: 0000-0002-5735-3857

Abstract: This paper is regarding the design, modeling and simulation for reducing harmonics with passive LLCL filter in off-grid solar system. It is desired that current and voltage waveforms are to be in the sinusoidal form during energy generation from stand-alone solar systems. This condition can be provided by the most important one of the main factors which to determine the quality of electrical energy. Due to the harmonics produced by the non-linear loads, the waveform of the current and voltage is distorted from the sinusoidal form. The passive LLCL filter is designed and analyzed for mitigation of the total harmonic distortion for current (THD$_I$) in the proposed off-grid PV system. The passive LLCL filter is practically installed between solar inverter and non-linear load. Simulation results are in a good compliance with the theoretical analysis. This study describes a design methodology of a LLCL filter for off-grid power system with a comprehensive study of how to mitigate the harmonics in off-grid solar system. The using of a LLCL filter mitigates the THD$_I$ that injected by a six pulse rectifier which is used as a non-linear load. The simulation result shows that the reduction of THD$_I$ from 89.89% to 3.257%. This paper attempts to show that the using of LLCL filter with a stand-alone solar system can highly improve the power quality of the system.

Keywords: *PV module model, Passive LLCL harmonic filter, Total harmonic distortion (THD), Off-grid PV system, Harmonic mitigation*

Nomenclature	
T	Temperature
G	Irradiance
PV	Photovoltaic
Voc	Open circuit voltage
Isc	Short circuit current
THD	Total harmonics distortion
THD$_I$	Total harmonics distortion for current
PWM	Pulse-width Modulation
LLCL Filter	Inductance-Inductance-Capacitor-Inductance Filter

1. INTRODUCTION

Photovoltaic (PV) cells are systems that convert solar energy directly into electrical energy without the need for any moving mechanism without polluting the environment, polluting the environment. PV system is safe and clean sources, and the use of these systems is increasing day by day. PV systems can be divided into two main field; off-grid or stand-alone applications and on-grid or grid-connected applications. Stand-alone systems can be used to provide energy for remote loads where the electric grid cannot access.

Design of an LLCL type filter for stand-alone PV systems' harmonics have been studied widely in the literatures. In [1] an efficient procedure was studied to design passive LCL-filters for active power filters. Thus, it was studied on the hybrid filters. However, our study is only on the mitigation of harmonics by LLCL filter in stand- alone PV system.

In [2] analytical solutions were investigated for LLCC filters connected in parallel resonant converters. In [3,4] elimination of harmonic components was studied by passive filter in electrical facilities, whereas in [5] harmonics elimination was investigated in grid-tie inverter. However, in some previous studies which were discussed about the design of an LLCL type filter for stand-alone PV systems' harmonics. In [6] optimum design of passive harmonic filter was studied by using game theory concepts. The authors concluded that choosing filter with using game theory concepts more important than other selections method.

Stand-alone PV systems are used in some power applications such as an electrical grid where is not existing, water pumps, communication stations, traffic signs, etc. [7,8]. The output voltage and current of solar inverter generally contain a lot of harmonic components as a result from the switching signals. Besides choosing a higher switching frequency to reduce the harmonic, the high frequency harmonic contents can be filtered by using active or passive filters. Principle scheme of a stand-alone PV system is as shown in Fig. 1.
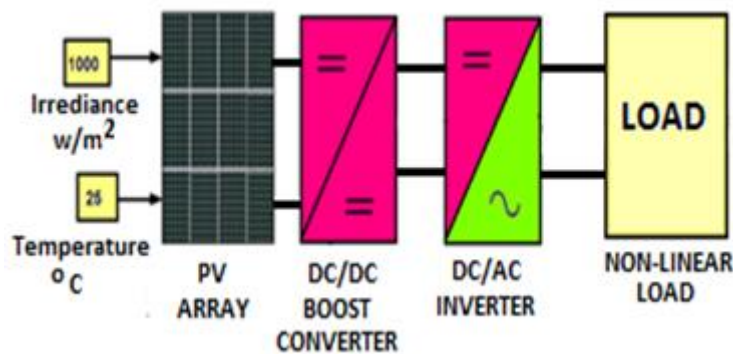
Figure 1. Principle scheme of stand-alone PV system (unfiltered)

The current and voltage waveforms away from the sinus form are distorted because the electrical loads do not have a non-linear characteristic. These results cause power quality problems due to harmonic components. Harmonic components cause many problems in power systems. They also have negative effects on photovoltaic sources and converters. Therefore, they should be mitigated. Converters are source of harmonics because of their switching elements, which have non-linear characteristics.

It is highly preferred to use passive filters to reduce harmonic components that occur in the solar PV system. Passive filters are used to reduce the input current of the total harmonic distortion (THD_I) of an uncontrolled rectifier. According to these results, the designed passive filters have a simple structure

and control is not too complicated provides significant advantages and are not complicated to control, which provides significant advantages. Passive filters are placed between source and load. Thus, they are designed to destroy components outside the basic component.

The use of passive filters in off-grid systems have many advantages such as including its small size, low cost and high performance. These filters are used for mitigation of harmonics occurred by both PWM inverters and low rated irradiation. They are also used to reduce harmonic components and improve the power quality in off-grid power systems. Passive filters must be used to keep the harmonic components at the limits specified in the standard.

The use of passive filters has many advantages, such as increasing the lifetime of the off-grid PV system, increasing in energy quality and improvement of the power factor value. The passive filters also reduce the value of harmonic components caused by six-pulse power converters, and solar inverter. Therefore, THD_I value drops significantly in the system.

On the other side the active harmonic filters have some disadvantages compare to passive filters such as they are complicated from technical wise, using of active filters are sophisticated in both electronics and software. Therefore, their maintenance is difficult and also manufacturer is being contacted usually for solution in any failure. In addition, active harmonic filters are always more expensive than passive harmonic filters.

Two types of filters are used in off-grid systems for harmonic mitigation, and can be classified into two main categories, passive and active filters. The active filters are much more complex, require active switches, and control algorithm. In recent years, LLCL filter has been widely used in renewable energy sources.

This energy is stored in the battery pack via the solar charge controller and is ready for use during day or night hours [3,9]. By adding a solar inverter to the system, the devices working with the mains voltage is fed. Panel slopes and orientations should be selected according to the season in which the energy will be consumed. The Principle scheme of stand-alone PV system is given in Fig.2.
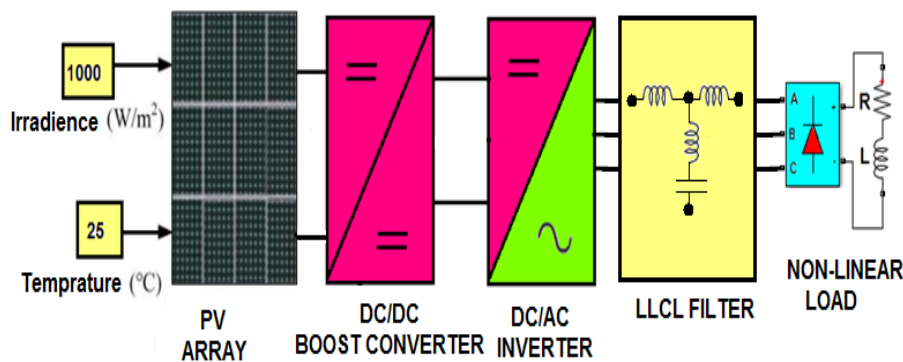
Figure 2. Principle scheme of stand-alone PV system (filtered)

All panels connecting to a charge controller should be on the same slope and orientation. The size of the PV array should be selected by some parameters such as seasonal variation of solar irradiation, cell temperature, the daily energy usage, battery efficiency, etc. [10,11]. The two main basic variables that can be set to the input of PV simulation system. These variables are the solar irradiation level W/m^2 and the module's temperature ºC.

Mitigation of harmonics will be achieved for the irradiation value 880 W/m^2 and the temperature is 20 ºC. The harmonics that occur in the stand-alone system change depending on the radiation and the

temperature [1,12]. This change has a nonlinear character, and the PV panels produce direct current electrical energy proportional to the temperatures and irradiance intensity.

In this paper, a six-pulse rectifier, which is used as a non-linear load, causes quite high value of THD_I in the stand-alone PV system. Therefore, passive LLCL filter is the most frequently used method for mitigation of THD_I in off-grid solar system. In this article, LLCL filter is designed and modeled for reduction of harmonics in stand-alone PV system. The proposed standalone PV system in this paper is formed as follows, a DC/DC boost converter, a solar inverter, an uncontrolled six pulse rectifier, a passive LLCL filter and an inductive R-L load.

According to the results obtained, harmonic problems still exist in the off-grid system that feeds a non-linear load and these problems should be solved. In this study, it was observed that this problem was mitigated and harmonics were cleaned significantly with LLCL type filter.

2. POWER SYSTEM HARMONICS IN OFF-GRID PV SYSTEM

The development of power electronics has led to an increase in harmonics in power system. The most important reason for the deterioration of the voltage waveform, the correlation between the terminal voltage and current with non-linear loads are non-sinusoidal sources. Even if nonlinear loads are low powering solar system, they distort sinusoidal current and voltage waveforms. Harmonics causing serious pollution problem in power system, and they also reduce the quality the energy give to the consumer. In addition, they cause transformer losses, line losses and resonance problems [2,13].

The six pulse converters, which used in off-grid PV system is the great harmonic source. Nonlinear loads create voltage and current harmonics, and these harmonics cause many problems. Six pulse rectifiers is used in off-grid PV system as a load [14]. The odd harmonics have greater impacts on power quality than even harmonics as they have higher magnitude. Harmonics generated by the converters may be formulated depending on the number of pulses of the converter. The harmonics produced by converters is calculated as:

$$h = kp \pm 1 \qquad (1)$$

Where, h is the harmonic component, k is positive integer number and p is number of the pulse converter. The odd-numbered harmonics are present in the six-pulse converter; but triple harmonics are not present in this converter. For example, 5th, 7th, 11th, 13th, 17th, 19th, 23rd, 25th, etc., are present as active in the six pulse uncontrolled rectifier. These harmonic components are as shown in the eq. [2].

$$
\begin{aligned}
i(\omega t) = {} & 14.88 Sin(\omega t - 0.159) + 2.98 Sin(5\omega t + 178.4) + 2.121 Sin(7\omega t - 179.2) \\
& + 1.348 Sin(11\omega t - 0.8763) + 1.14 Sin(13\omega t - 0.4928) + 0.8717 Sin(17\omega t \\
& + 178.7)
\end{aligned} \qquad (2)
$$

These harmonic components waveform is as illustrated in Fig.3.
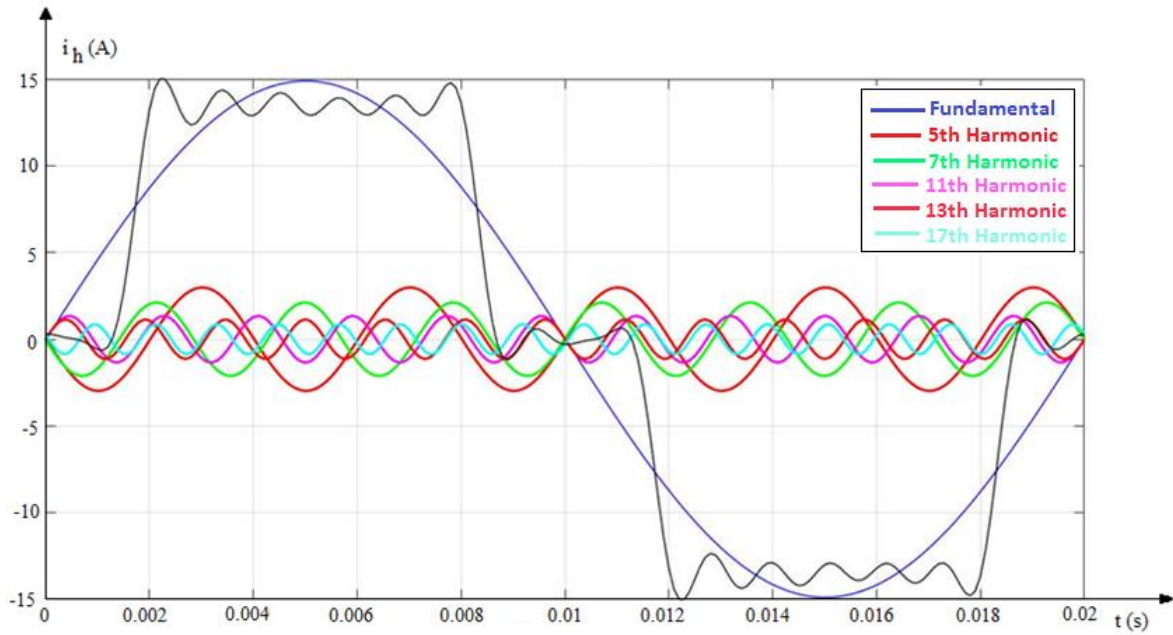
Figure 3. Six-pulse rectifier input current harmonics waveform

Current and voltage that is in the sinusoidal waveform distorted by non-linear, loads that even if they are in small power. Harmonic components cause the following damages in the PV system such as; Increased losses of elements in the off-grid PV system. Disruption of the dielectric insulation of elements in the power system, increase in voltage drop in off-grid PV system and inconstant voltage level, incorrect measurements on measurement systems, disorders in control circuits.

Resonance with harmonics component, Incorrect opening in protection relays, Incorrect operation of microprocessors and data loss, Noise in communication devices, change of power factor, Overheating and power loss of power system equipment such as cables, AC/DC converters, inverter, six pulse rectifier and inductive R-L load, shortened life span of off-grid system devices such as cables, DC/DC boost converter, and inverter, false trigger switching elements such as Insulated-Gate Bipolar Transistor (IGBT), Metal Oxide Semiconductor Field Effect Transistor (MOSFET), Bipolar Junction Transistor (BJT) and etc., errors measurements voltage, current and power in off-grid PV system.

Harmonics must be continuously monitored for power quality. THD_I or total harmonic distortion for current is a common measurement of the level of harmonic distortion present in electrical power system [4,5]. In order to be able to measure the energy quality and classify the distortions, it is necessary to define the total harmonic distortion. The THD_I term expresses as effective value of the all harmonics, divide by the effective value of its fundamental of current. We can determine the level of damage harmonics giving to the network by the THD coefficient. The distortion as a percentage of total harmonic distortion for current is defined as follow:

$$THD_I = \frac{\sqrt{\sum_{n=2}^{\infty} I_n^2}}{I_1} \qquad (3)$$

Where, I_n effective current of the nth harmonic, I_1 is the effective of the current of the fundamental frequency. The high THD have negative effects on power system such as equipment overheating, motor vibration, neutral overloading and low power factor. THD_I or total harmonic distortion for current is a common measurement of the level of harmonic distortion present in power system. If the harmonics components are equal to the "0", total harmonic distortion will be equal to the "0" where, In, is the effective voltage of nth harmonic and n=1 is voltage of the fundamental frequency [6, 15]. The analytical solutions and simulation program applications have been observed that fit harmonics occur in the electrical grid system, any or both of these sources of non-sinusoidal nonlinear elements in general.

There are many damages is given by harmonics to off-grid PV system such as excessive current in neutral wire, overheating of the DC/DC boost converter, microprocessor problem and unexplained inverter crash. The presence of harmonic currents and voltages of the power system means that the degradation of sinusoidal waves. Deteriorated waves called non-sinusoidal waves [16]. Voltage and current waveform distortion due to harmonics can lead to the power system and electrical consumer either damaged or out of order.

Some non-linear loads cause harmonics in off-grid solar system such as switched power supplies, control circuits, battery chargers, solar inverters, DC/DC converter, DC/AC rectifier, PV systems. Although capacitors themselves do not produce harmonics, they are one of the elements most affected by harmonics. The harmonic effect is usually observed in parallel-connected capacitor groups.

There are two commonly used methods for destroying harmonics. One of these measures taken during the design phase of the power system, the other circuit elements such as L, C, and L are added to circuit. In order to mitigate the harmonics, these elements are called "harmonic filter" which enables to mitigate the harmonic components that are formed by the nonlinear elements which are present in the circuit. Over voltages and currents that occur as a result of the resonance phenomenon generated by the harmonics.

Harmonics cause additional heat losses in the off-grid energy system. This additional loss reduces the efficiency of the system. It is impossible to destroy the harmonics. Measures will be taken to minimize harmonics. For example, rectifiers can be selected with 12 pulses instead of 6 pulses. These measures are not enough to filter absolutely necessary.

The general purpose of the harmonic filter to reduce the effects of current and voltage in the designated frequency. In parallel with the developments in the power electronics, many nonlinear loads are connected to the power system. It may be possible to filter harmonics with passive filters consisting of L, R, C elements.

3. ANALYSIS AND DESIGN OF LLCL PASSIVE FILTERS

Working of electricity systems smoothly and safety depends on the foundation of quantities such as current and voltage which are sinusoidal and 50 Hz frequency However, these foundation quantities lose their sinusoidal characteristics because of many reasons, and unwanted harmonics occur in the system. The DC / DC boost converter, DC/AC inverter and six-pulse uncontrolled converter are harmonics sources which use in the off-grid PV system.

This study focuses on the design and analysis of LLCL passive filters for improvement power quality in off-grid PV systems. In the last decade, owing to the quick growth of renewable energy in the world, the LLCL filter has been used extensively for various applications in renewable energy sources. Harmonic currents generated by power electronic based devices such as thyristor, diode, MOSFET and IGBT these elements cause critical power quality problems in the PV systems.

Having more THD during low solar irradiation might force PV system operators to either use bigger and more expensive filters or even disconnecting the PV system from the grid to avoid paying the high THD levels penalty specified by the utility operator. As a result, the use of these nonlinear elements increases the effectiveness of the harmonics in the system. In addition, rectifiers, inverters, DC/DC converter are the most significant harmonic sources in off-grid power system. This problem occurs around resonance frequency Fig.4. Shows the frequency response of LLCL filter.
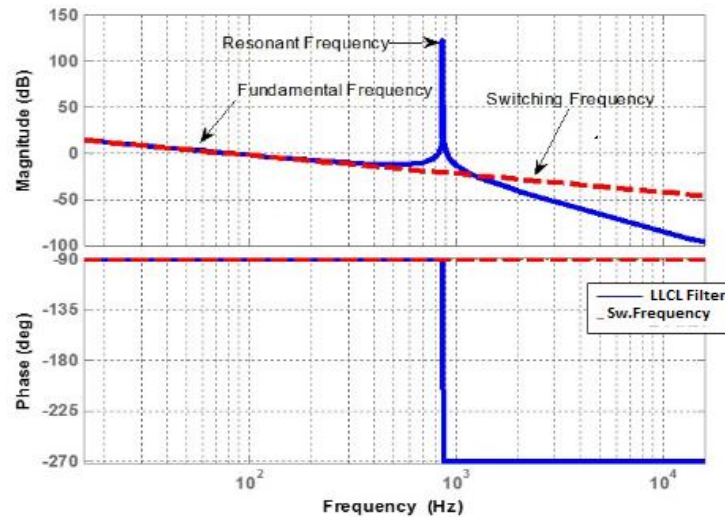
Figure 4. Frequency response of LLCL filter

The harmonic filters are designed so that the current or voltages at one or more frequencies to reduce or mitigate the effect of the harmonic level. Generally, designs are made for the most effective harmonic components. In fact, the reason for using filters is both technical and economical. It is aimed to mitigate the technical and economical disadvantages resulting from the harmful effects of the harmonics with the filters.

Passive LLCL filter is circuits consisting of capacitor C_f, inductance L_1, inductance L_2 and inductance L_f elements, which is placed between the solar inverter and load. Thus, they are designed to mitigate harmonics components outside the fundamental frequency. A passive LLCL filter has a lot of advantages over an active filter such as guaranteed stability, no power consumption, inexpensive, and conventional. Input voltage of solar inverter is given in Fig. 5.
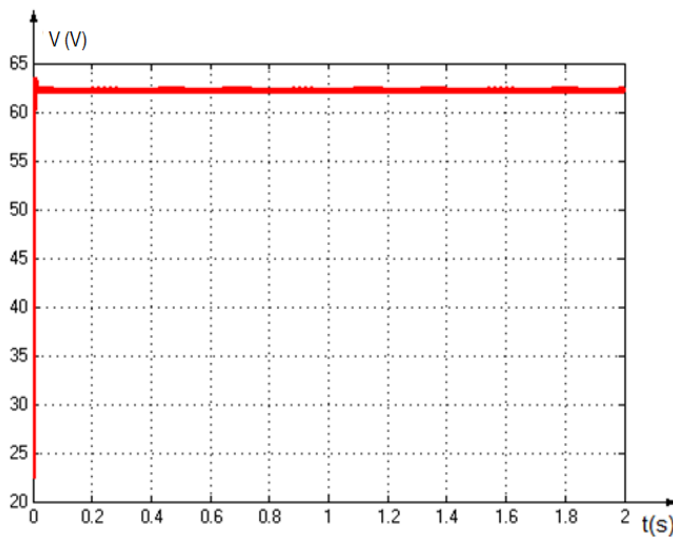
Figure 5. Input voltage of solar inverter

Passive LLCL-filter is usually used on the load side of renewable energy sources, such as wind energy, PV energy etc. These devices improve and ensure the overall quality energy produced by off-grid PV system. Schematic diagram of the LLCL filter is as illustrated in Fig.6.
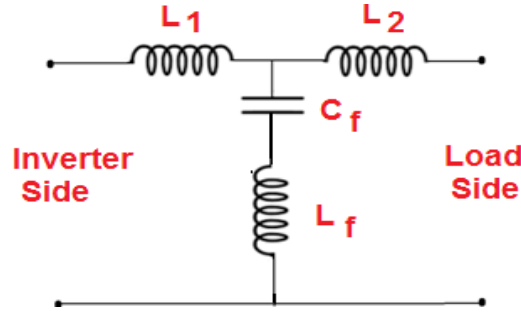
Figure 6. Schematic diagram of LLCL filter

Passive LLCL filter is used to reduce harmonics and improvement power quality in off-grid power system. This filtering is based on the principle of mitigating harmonic components in the network by adjusting the L-C passive elements. The structure of these filters being simple, low prices, high efficiency and being able to meet basic frequency reactive power needs at the same time the ones of this filters advantages. LLCL filter is become popular in the renewable energy industry nowadays, but it can only be used in systems with fixed nonlinear loads.

A passive LLCL harmonic filter should be designed correctly for stand-alone PV system. A passive LLCL filter can be designed for purposes such as harmonic current spectrum of harmonic generating nonlinear loads, the value of the total harmonic distortion allowed in the solar system, reactive power value required in solar system, level of harmonics caused by other sources, the other loads in the network and the equivalent circuit of the solar system impedance change for effective harmonics, working values of the filtration (frequency, temperature, voltage).

The value of a filter is the fundamental frequency of this filter is defined as the reactive power that it provides. This is equal to the value of the fundamental reactive power provided by the capacitors. The filter should be positioned nearest to the harmonic load.

The resonance event is one of the harmonic components or close to these harmonic components the values of the harmonic current and voltage values reach very large levels Therefore, by adjusting the filter resonant frequency is shifted. It provides an efficient way to improve the quality of power fed from off-grid PV system to the inductive R-L load. As shown in Fig. 6, the LLCL filter circuit consists of on the inverter side inductance L_1, on the load side inductance L_2 and a capacitor C_f the LLCL filter transfer function is as given below.

$$G(j\omega) = \frac{L_f C_f s^2 + 1}{[L_1 L_2 C_f + (L_1 + L_2)C_f]s^3 + (L_1 + L_2)s} \qquad (4)$$

The resonant frequency of the LLCL filter should be chosen in the range given below. When selected in this range, no resonance occurs in the off-grid solar system.

$$10\,\omega_0 \leq \omega_{res} \leq (\omega_{switch}/2) \qquad (5)$$

Where w_0 is the utility frequency rad/s, W_{res} is the resonant frequency rad/s and W_{switch} is the switching frequency rad/s. The resonant frequency of LLCL filter at the switching frequency is defined as:

$$f_{res} = \frac{1}{2\pi * \sqrt{(\frac{L_1 L_2}{L_1 + L_2} + L_f)C_f}} \qquad (6)$$

If we choose C_f large value, we can mitigate more harmonic, but it results in higher reactive power and increased demand of current from L_1 thereby decreasing the efficiency of the overall filter system. Reactive power absorbed by capacitor is defined as:

$$Q_c = \frac{3V_{rated}^2}{X_c} = \frac{3V_{rated}^2}{\frac{1}{\omega\,c}} = 3(2\pi f)C_f V_{rated}^2 \leq \alpha P_{rated} \tag{7}$$

Where Qc is reactive power absorbed by capacitor. V_{rated} is effective value of phase voltage. α is reactive power absorption rate. It is generally chosen as given below.

$$\alpha < 5\% \tag{8}$$

LLCL filter is occurred three inductors and one capacitor. The capacitor shunt element in the design will further attenuate the switching frequency. The C_f value for the LLCL filter is chosen by determining the reactive power absorbed by the filter at rated conditions [7]. Eq. [9] determines the selection of C_f value for the LLCL filter.

$$C_f = \frac{\alpha P_{rated}}{3(2\pi f)V_{rated}^2} \tag{9}$$

The inductors in the LLCL filter are designed by determining the current ripple. Selection of small values of ripple current decreases the switching losses. However, the size of the inductor increases. The value of L_1 in LLCL filter is defined as

$$L_1 = \frac{N_{in}}{8hf_{res}} \tag{10}$$

Where V_{in} is the input voltage of the inverter, h is the amount of ripple current which should be 5% of rated current. The value of L_2 is defined as

$$L_1 = aL_2 \tag{11}$$

Where, a is the inductance ratio factor. For low and medium power applications, this coefficient is chosen to be greater than 1. Passive LLCL filters are placed between the source and the load and they are designed to destroy components outside the basic component. These filters have risks such as serial and parallel resonance, the filtering frequency is fixed, and being large volumes disadvantages of these filters.

$$L_f = \frac{1}{C_f\,\omega_{s\omega}^2} \tag{12}$$

Harmonics are undesirable magnitudes in the network because they affect all system elements. Therefore, it is electrical network. Band pass and high-pass filters are frequently used.

4. MITIGATION OF HARMONICS USING PASSIVE LLCL FILTER

The irradiation and temperature are taken as 880 W/m^2 and 20 ºC in stand-alone PV system. The Point of Common Coupling (PCC) will be the focus of analysis which THD$_I$ is limited less than 5%. It is clear that the THD$_I$ of the current of inverter is 89.89 %. Higher order harmonics can affect whole of the system.

These effects reduce the performance of the power system and other equipment. Simulation model of the proposed system is simulated in a software program as shown in Fig. 7. Simulation program was used to analyze performance of the designed passive LLCL filter in stand-alone PV system. The model of stand-alone PV system (unfiltered) is also given in Fig.7.
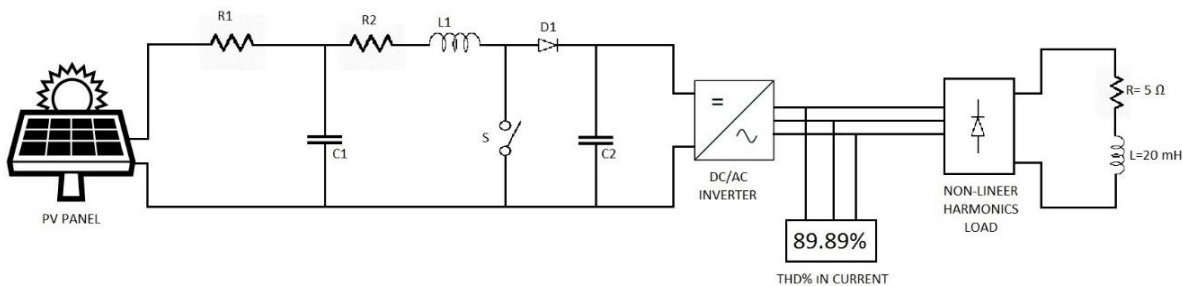
Figure 7. Model off-grid PV system (unfiltered)

A Simulation program was used to analyze performance of the designed passive LLCL filters. Harmonics which are produced by non-linear loads must not resonate the PV system. Resonance conditions should be calculated separately for each harmonic component. If harmonics are injected into a power system from harmonic sources, they affect the PV system in such a way that it will resonate with any component. The output voltage waveform of stand-alone system is given in Fig.8.
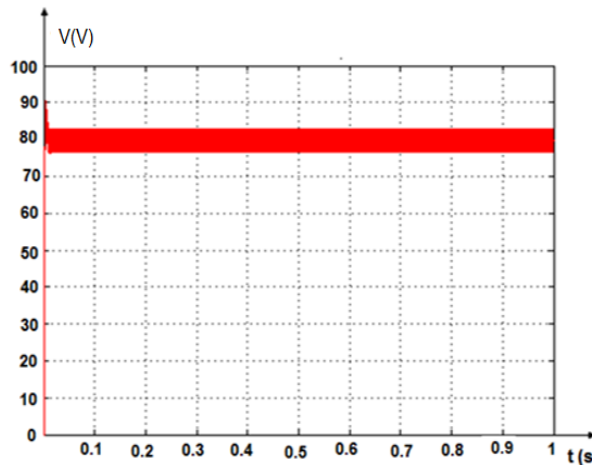
Figure 8. The output voltage waveform of Stand-alone System

Passive LLCL filters are generally used in power systems. The reason for this is that the cost is lower than the active filter and easy to use. The dominant harmonics are detected in the power system and the passive LLCL filter is designed accordingly. While harmonic compensation is made with passive LLCL filter, and the reactive power compensation is also performed.

System structure and working modes are analyzed in detail firstly, and then THD$_I$ belongs to the power system analysis based on the simulation program. The results clearly show that the passive LLCL filter can reduce harmonics at various frequencies as compared to active filter. The inverter output currents

waveform for unfiltered condition is shown in Fig.9.
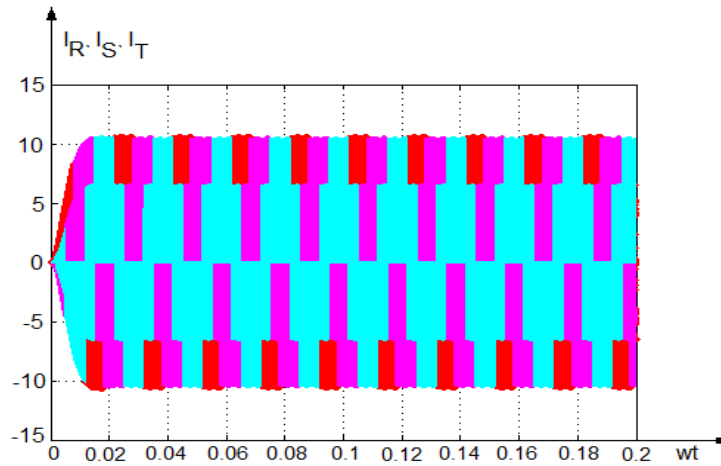
Figure 9. Inverter output currents waveform (without filter)

Harmonics have two effects on stand-alone PV systems, technical and economical. Technical problems affect the delivery of quality electricity to the load. Economic problems affect optimal work. Fig. 10, shows the schematic diagram of the power system after filtering. In this system, LLCL filter is used to mitigate all of the harmonics. In this paper, stand-alone PV power system has been simulated with and without passive filters in the Simulation software program. Parameter values of the LLCL filter values obtained from Eqs. [9,10] are given in Table 1.

Table 1. Designing parameters of LLCL filter

Parameters of LLCL filter	Values
Cf	115.55 µF
L1	258.19 mH
L2	314.55 mH
Lf	140.4 µF

Higher order harmonics can affect the whole stand-alone system. These effects reduce the performance of the power system and other equipment. There are odd and even harmonics in off-grid PV systems. THD values vary with high and low radiation values. It has been observed that THD value increases at low radiation. The simulation results show that the odd harmonics components are contributed to more harmonics as compared to even harmonics. It also shows that THD_I value has come down to 3.257 %.

Passive LLCL filter is placed between solar inverter and the load. They are designed to destroy components outside the basic component. These filters have risks such as serial and parallel resonance, the filtering frequency is fixed, and being large volumes disadvantages of these filters. Harmonics are undesirable magnitudes in the network because they affect all system elements.

The increase of power electronic elements and various nonlinear elements every day causes the increase of the non-sinusoidal size circulating in the energy system. Therefore, it is necessary to establish filter circuits to mitigate harmonics. For this reason, filters are installed in renewable energy sources. Band pass and high-pass filters are frequently used. Model stand-alone PV system with filter is given in Fig.10.
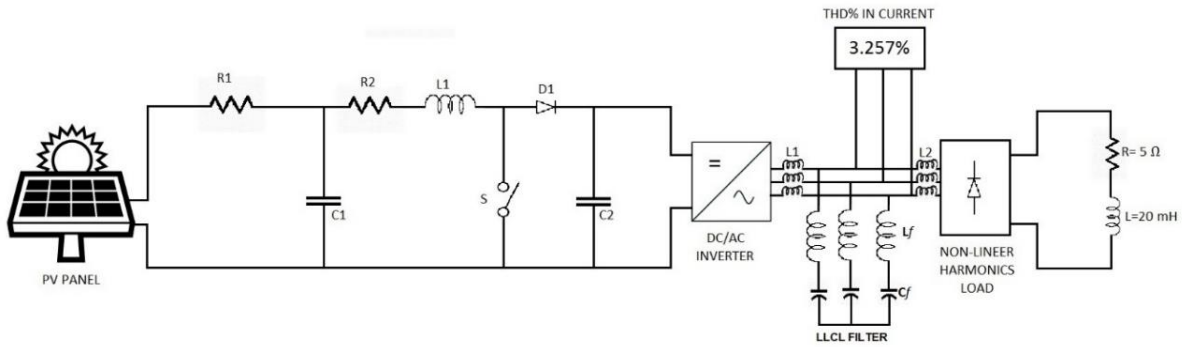
Figure 10. Off-grid PV system model with LLCL filter

This paper presents the passive LLCL filter application is to mitigate harmonics and improve the power quality of the off-grid PV system. Simulations are performed to see what affects the harmonics on the system waveform and what kind of problems will be solved. Thus, we have used passive LLCL filter to mitigate harmonics in PV system. LLCL filter is especially popular in the renewable systems. This filter has many advantages like small losses, small size and weight. The output voltage of DC/DC boost converter waveform is as shown in Fig. 11.
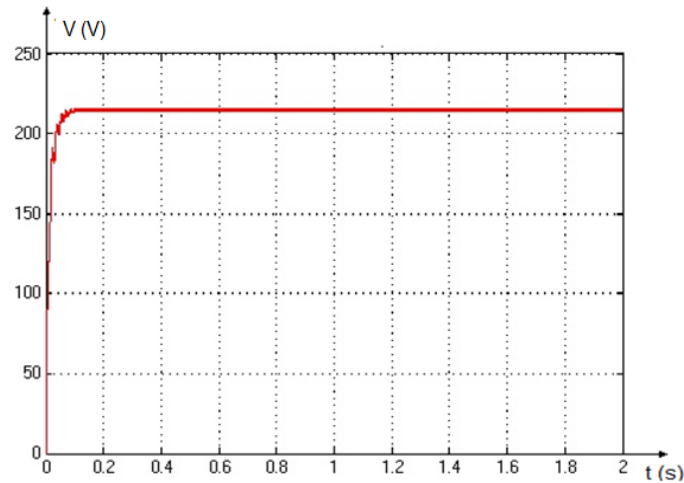
Figure 11. Output voltage of DC/DC boost converter

Harmonics cause additional losses in energy cable, motors, capacitors and transformers. In some cases, harmonics cause the power system components to breakdown or be disabled. They will also increase the probability of occurrence of resonance, and over-currents and voltages that may occur as a result of resonance will cause great damage to the operating elements. The THD$_I$ has been successfully decreased from 89.89 % to 3.257 % for the used non-linear load system, which fulfills the recommended (IEEE-519).

LLCL filter has been commonly used to limit the flow of harmonic currents in stand-alone PV system. They are usually custom designed for the application. However, their performance is limited to a few harmonics and they can introduce resonance in the stand-alone system. The idea of using passive LLCL filter is to compensate for current and voltage harmonics in off-grid PV system. The passive LLCL filter plays rather an important role in reducing system harmonics for better quality energy, but the main drawback of the LLCL filter is a stability problem.

Working of electricity systems smoothly and safety depends on the foundation of quantity effects such as current and voltage, which are sinusoidal and 50 Hz frequency. However, these foundation quantities lose their sinusoidal characteristics because of many reasons, and unwanted harmonics occur in the system. These harmonics which are occurred on the current and voltage waves can damage electricity installation and consumers depended on them.

The most common ways to reduce them in order to take precautions such as larger neutral conductor section, using of K-factor transformers, using passive LCL filters, with some transformer connections some harmonics can be eliminated. For example, delta-star transformer connection eliminates 5th and 7th harmonics, delta-star transformer connection eliminates 3rd harmonic, 5th harmonic is destroyed by transformer with delta-zigzag connection, using a passive filter to neutralize triple harmonics in the neutral conductor, using high- pulse converters.

There are many serious effects of harmonics in the power system such as distortions of voltage waveform, decrease system efficiency and increase losses in the system. One of the most important harmonic components in energy systems is single and three phase converters. Harmonics should be drawn below the values stated in standards.

Non-linear elements cause serious harmonic pollution in stand-alone PV system and decrease the quality of energy given to load. Mitigation of harmonics and improvement of the power quality is essential this work. Harmonic filters cause temperature increase in the panel. Therefore, care should be taken to ensure that the panels provide adequate airflow. As a result of LLCL passive filter application the system was cleaned from harmonics and the THD_I value fell below 5%. As the system losses decreased, efficiency increased. It is clear that the THD_I has drawn to 3.257 %. PV system model with LLCL filter the output currents of solar inverter waveform is as shown in Fig. 12.
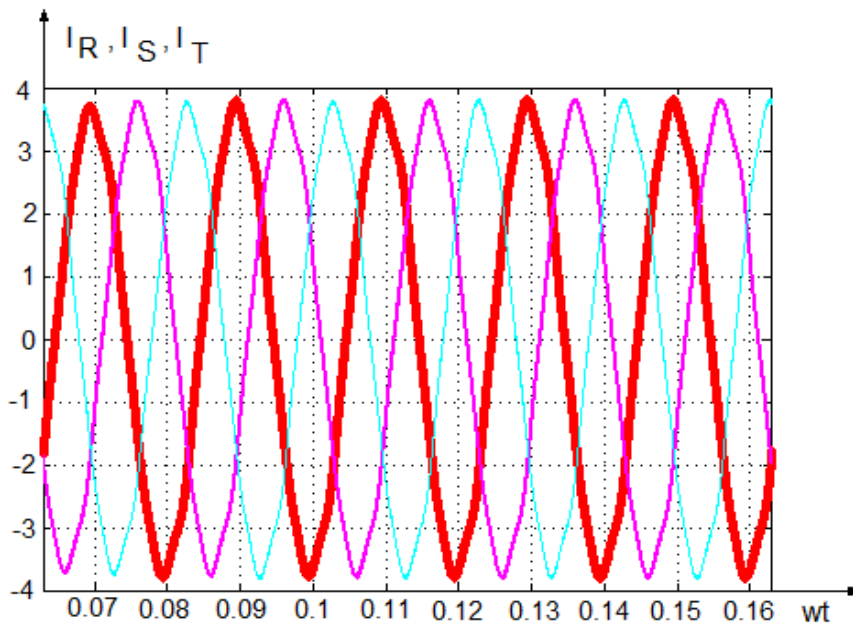
Figure 12. Output currents of solar inverter (after filtering)

The development in renewable energy over time has increased the demand for LLCL filters, which are an efficient and economical way of ensuring and improving the quality of power fed from the stand-alone PV system to load. Traditionally passive LLCL filters are used to mitigate line current harmonics. However, in practice, these passive filters have some disadvantages such as serial and parallel resonance.

One of the biggest harmful effects of harmonics is resonance effect, and the resonance occurs if the inductive reactance is equal to the capacitive reactance. As the frequency increases in the power systems, the inductive reactance increases, the capacitive reactance decreases. In the case of resonance, current and voltages are generated in the circuit at the excessive level.

5. RESULTS AND DISCUSSION

The power system consists of PV array, DC/DC boost converter, DC/AC solar inverter, passive LLCL filter, six pulse uncontrolled rectifier and inductive R-L loads. The design of passive LLCL filters to mitigate harmonic distortion caused by nonlinear loads in off-grid PV system. Mitigation of harmonics is so important for the power quality of stand-alone PV system. Passive LLCL filter is an effective filter to suppress high-level frequency components that are generated by PWM converter and non-linear loads.

The LLCL passive filter has the risk of resonance with the 5., 7., and 11., harmonic components in the PV system. The risk can be reduced partially by connecting a series resistor in the LLCL passive filter. It is convenient to use an LLCL passive filter in the Stand-alone PV systems. In addition, it is much more economical comparing to active filters.

There are some disadvantages for LLCL passive filters such as their sizes are big and they cannot fulfill the requirements in case of load changes then the parameters (L-C-L) should be changed based on the load. The aim is to mitigate such these negative effects for researchers who study in passive filters will be achievement.

In order to provide a constant output voltage for the six-pulse uncontrolled rectifier, a band-pass LLCL circuit has been applied. Especially in rectifier circuit applications, the LLCL filter gives better results. As a result of using the passive LLCL filter in the stand-alone PV system, THD_I reduced from 89.89 % to 3.257 %. These values correspond to the values expressed by the standards.

LLCL filters have some problems such as stability and resonance. It should be concentrated especially on these problems in order to get desirable results for the future.

REFERENCES

[1] Tavakoli, BM, Pashajavid, E. An efficient procedure to design passive LCL-filters for active power filters. Electric Power Systems Research, 2009, 79, 606-614. DOI: 10.1016/j.epsr.2008.08.
[2] Cheng, JH, Witulski, A. Analytic solutions for LLCC parallel resonant converter simplify use of two and three-element converters. IEEE Transactions on Power Electronics, 1998, 13, 235–243.
[3] Yilmaz, AS, Alkan, A, Asyali. MH. Applications of parametric spectral estimation methods on detection of power system harmonics. Electric Power Systems Research, 2008, 78, 683-693. Doi.org/10.1016/j.epsr.2007.05.011.
[4] Rüstemli S, Okuducu E, and Efe SB. Elektrik Tesislerinde Harmoniklerin Pasif Filtre Kullanılarak Azaltılması ve Simulasyonu (in Turkish). In: EVK2015 6. Energy Efficiency and Quality Symposium ; 4-6 June 2015 : pp 120-124.
[5] Xing Z, Hong Z, Fei L, Fang L, Chun L, Benxuan L. An LCL-LC power filter for grid-tied inverter. In: TENCON IEEE Region 10 Conference; October 2013: pp. 1-4.
[6] Rashid, HM. Power Electronics, Circuits, Devices, and Applications, USA: Pearson Press, 2014.
[7] Zhou, F, Luo A, Li, Y, Xu, Q, He, Z, Guerrero, JM. Double-carrier phase-disposition pulse width modulation method for modular multilevel converters. Energies, 2017; 10: 581–704. Doi:10.3390/en10040581.
[8] Er, Z, Balci, E. Dual axis solar angle tracking system without any sensor. Journal of Energy Systems, 2018, 2, 127-136. Doi.org/10.30521/jes.379164.
[9] Kececioglu, OF, Acikgoz, H, Yildiz, C, Gani, A, Sekkeli, M. Power Quality Improvement Using Hybrid Passive Filter Configuration for Wind Energy Systems. Journal of Electrical Engineering Technology, 2017, 12, 2370-2375. DOI: 10.1016/j.sbspro.2015.06.211

[10] Ozdemir, A, Ferikoglu, A. Low cost mixed-signal microcontroller based power measurement technique. IEE Proceedings-Science Measurement and Technology, 2004, 151, 253-258. Doi: 10.1049/ip-smt:20040242 – JUL.

[11] Cangi H, Adak S. Analysis of solar inverter THD according to PWM's carrier frequency. In: International Conference on Renewable Energy Research and Applications (ICRERA); November 2015: DOI: 10.1109/ICRERA.2015, 7418694.

[12] Ang, Y, Bingham, C, Foster, M, Howe, D. Design oriented analysis of fourth-order LCLC converters with capacitive output filter. IEE Proceedings -Electric Power Applications, 2005, 152, 310–322, 2005. DOI: 10.1049/ip-epa:20045112

[13] Adak, S, Cangi, H. Analysis and Simulation Total Harmonic Distortion of Output Voltage Three Level Diode Clamped Inverter in Photovoltaic System. Bitlis ErenUniversity Journal of Science, 2015, 5, 2147-3129.

[14] Olalla, C, Clement, D, Rodriguez, M, Maksimovic, D. Architectures and Control of Submodule Integrated DC–DC Converters for Photovoltaic Applications. IEEE Trans. Power Electronics, 2013, 28, 2980–2997, DoiI: 10.1109/TPEL.2012.2219073.

[15] Hayes J, Egan M. Rectifier-compensated fundamental mode approximation analysis of the series parallel LCLC family of resonant converters with capacitive output filter and voltage-source load. In: 30th Annual IEEE Power Electronics Specialists Conference PESC 99; 1999: pp. 1030–1036.

[16] Dastfan, A, Yassam, H, Rafiei, MR. Optimum Design of Passive Harmonic Filter by Using Game Theory Concepts. Intelligent Systems in Electrical Engineering, 2014, 4, 13-22.